Systems/Circuits

Neuronal Switching between Single- and Dual-Network Activity via Modulation of Intrinsic Membrane Properties

Savanna-Rae H. Fahoum and Dawn M. Blitz
Department of Biology and Center for Neuroscience, Miami University, Oxford, Ohio 45056

Oscillatory networks underlie rhythmic behaviors (e.g., walking, chewing) and complex behaviors (e.g., memory formation, decision-making). Flexibility of oscillatory networks includes neurons switching between single- and dual-network participation, even generating oscillations at two distinct frequencies. Modulation of synaptic strength can underlie this neuronal switching. Here we ask whether switching into dual-frequency oscillations can also result from modulation of intrinsic neuronal properties. The isolated stomatogastric nervous system of male *Cancer borealis* crabs contains two well-characterized rhythmic feeding-related networks (pyloric, ~1 Hz; gastric mill, ~0.1 Hz). The identified modulatory projection neuron MCN5 causes the pyloric-only lateral posterior gastric (LPG) neuron to switch to dual pyloric/gastric mill bursting. Bath applying the MCN5 neuropeptide transmitter Gly^1-SIFamide only partly mimics the LPG switch to dual activity because of continued LP neuron inhibition of LPG. Here, we find that MCN5 uses a cotransmitter, glutamate, to inhibit LP, unlike Gly^1-SIFamide excitation of LP. Thus, we modeled the MCN5-elicited LPG switching with Gly^1-SIFamide application and LP photoinactivation. Using hyperpolarization of pyloric pacemaker neurons and gastric mill network neurons, we found that LPG pyloric-timed oscillations require rhythmic electrical synaptic input. However, LPG gastric mill-timed oscillations do not require any pyloric/gastric mill synaptic input and are voltage-dependent. Thus, we identify modulation of intrinsic properties as an additional mechanism for switching a neuron into dual-frequency activity. Instead of synaptic modulation switching a neuron into a second network as a passive follower, modulation of intrinsic properties could enable a switching neuron to become an active contributor to rhythm generation in the second network.

Key words: **central pattern generator; internetwork coordination; network recruitment; neuromodulation; neuropeptide**

Significance Statement

Neuromodulation of oscillatory networks can enable network neurons to switch from single- to dual-network participation, even when two networks oscillate at distinct frequencies. We used small, well-characterized networks to determine whether modulation of synaptic strength, an identified mechanism for switching, is necessary for dual-network recruitment. We demonstrate that rhythmic electrical synaptic input is required for continued linkage with a "home" network, whereas modulation of intrinsic properties enables a neuron to generate oscillations at a second frequency. Neuromodulator-induced switches in neuronal participation between networks occur in motor, cognitive, and sensory networks. Our study highlights the importance of considering intrinsic properties as a pivotal target for enabling parallel participation of a neuron in two oscillatory networks.

Introduction

Oscillatory networks are important for rhythmic motor behaviors, such as locomotion, and complex behaviors, such as memory processing (McCormick and Bal, 1997; Buzsáki, 2002; Wang, 2010; Bucher et al., 2015). Individual neurons can participate in more than one rhythmic network, and even oscillate at multiple frequencies simultaneously. This includes neurons bursting in time with breathing and vocalizing, or other orofacial networks, with multiple feeding networks, and with multiple hippocampal or cortical rhythms (Steriade et al., 1993; Dickinson, 1995; Roopun et al., 2008; Bartlett and Leiter, 2012). However, multiplexing of neuronal activity across networks is not a static feature.

Network flexibility extends to neurons switching participation between networks (Dickinson, 1995; Bouret and Sara, 2005; Koch et al., 2011). This "neuronal switching" includes neurons being recruited into or removed from a network; neurons from multiple networks joining together into a single, novel network;

Received Jan. 26, 2021; revised July 26, 2021; accepted July 28, 2021.

Author contributions: S.-R.H.F. and D.M.B. designed research; S.-R.H.F. and D.M.B. performed research; S.-R.H.F. analyzed data; S.-R.H.F. wrote the first draft of the paper; S.-R.H.F. and D.M.B. edited the paper; S.-R.H.F. and D.M.B. wrote the paper.

This work was supported by National Science Foundation IOS1755283 to D.M.B. We thank Dirk Bucher for assistance with spectral analysis; and Ryan Snyder for contributing several experiments and for helpful discussions and feedback on the manuscript.

The authors declare no competing financial interests.

Correspondence should be addressed to Dawn M. Blitz at Dawn.Blitz@MiamiOH.edu.

https://doi.org/10.1523/JNEUROSCI.0286-21.2021

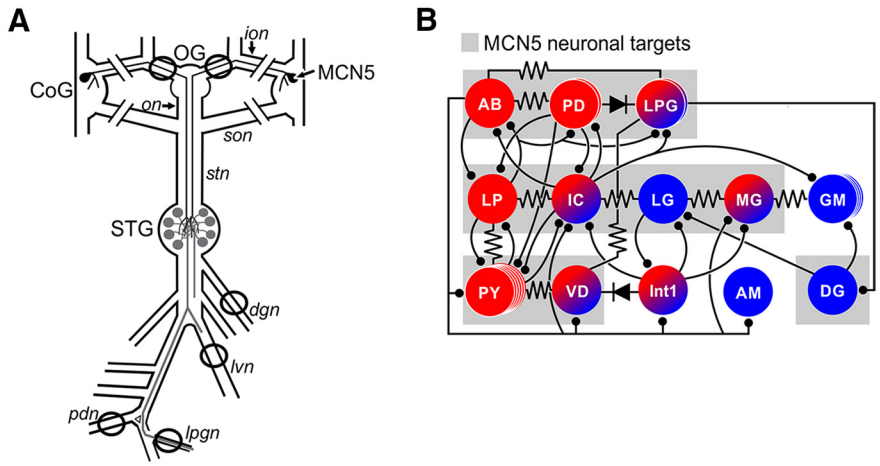

Figure 1. Schematic of the isolated STNS, including modulatory projection neuron MCN5 and connectivity of pyloric and gastric mill networks. ***A***, The isolated STNS is comprised of the paired commissural ganglia (CoG), oesophageal ganglion (OG), and STG, as well as their connecting and peripheral nerves. A single MCN5 projects from each CoG through the *ion, on,* and *stn* to the STG (Norris et al., 1996). The line breaks on the *sons* and *ions* indicate where these nerves were cut to isolate the STG networks (see Materials and Methods). Black circles on nerves represent locations of extracellular recordings. ***B***, The related pyloric and gastric mill networks have extensive electrical (resistor and diode symbols) and chemical inhibitory (ball and stick) connections between network neurons. Some neurons are exclusively active with the pyloric network (red), some exclusively with the gastric mill network (blue), and some can be active with both networks (red/blue) under different modulatory conditions. MCN5 acts on most STG neurons (gray backgrounds), including inhibiting the PY and LP neurons, exciting the pyloric pacemaker ensemble (AB, PD, LPG), and activating the gastric mill neurons IC, LG, and DG (Norris et al., 1996; Blitz et al., 2019). Ganglia: CoG, commissural ganglion; OG, Oesophageal ganglion; STG, stomatogastric ganglion. Nerves: *dgn*, dorsal gastric nerve; *ion*, inferior oesophageal nerve; *lpgn*, lateral posterior gastric nerve; *lvn*, lateral ventricular nerve; *on*, oesophageal nerve; *pdn*, pyloric dilator nerve; *son*, superior oesophageal nerve; *stn*, stomatogastric nerve. Neurons: AB, anterior burster; AM, anterior median; DG, dorsal gastric; GM, gastric mill; IC, inferior cardiac; Int1, interneuron 1; LG, lateral gastric; LP, lateral pyloric; LPG, lateral posterior gastric; MCN5, modulatory commissural neuron 5; MG, medial gastric; PD, pyloric dilator; PY, pyloric; VD, ventricular dilator.

or neurons switching between single- and dual-network participation (Dickinson et al., 1990; Hooper and Moulins, 1990; Meyrand et al., 1994; Weimann and Marder, 1994; Tryba et al., 2008; Koch et al., 2011). Small invertebrate motor systems enable identification of modulatory projection neurons as endogenous sources of neuromodulators that elicit neuronal switching (Meyrand et al., 1994; Faumont et al., 2005). Based on invertebrate and systems-level vertebrate studies, it is proposed that modulatory neurons in vertebrate nervous systems similarly elicit neuronal switching (Bouret and Sara, 2005). For example, exogenous modulators elicit switching in respiratory networks (Tryba et al., 2008), noradrenergic signaling regulates coupling of brain regions during stress responses in human fMRI measurements, and locus coeruleus activation elicits cognitive shifts and large-scale connectivity changes in rodents and monkeys (Bouret and Sara, 2005; Hermans et al., 2011; Zerbi et al., 2019). However, it is difficult to selectively manipulate modulatory neurons and identify the cellular mechanisms of neuromodulator-elicited neuronal switching in large diffuse networks.

In general, neuromodulators alter the intrinsic membrane properties of neurons and/or the synapses between them (Harris-Warrick, 2011; Marder et al., 2014; Nadim and Bucher, 2014). In invertebrate networks, modulation of synaptic strength is necessary for recruiting switching neurons between networks (Hooper and Moulins, 1990; Meyrand et al., 1994). Although work in larger vertebrate networks and computational studies suggest that modulation of intrinsic membrane properties also contributes to switching (Tryba et al., 2008; Drion et al., 2019), complications, such as electrical coupling, have prevented confirming this in a biological context. Further, it remains unknown whether intrinsic properties can be sufficient to enable neuronal switching into a second oscillation frequency.

To study neuronal switching, we used the isolated stomatogastric nervous system (STNS) of the crab *Cancer borealis*, which contains identified modulatory inputs that alter well-defined networks (Stein, 2009; Marder, 2012; Daur et al., 2016). The STNS includes two networks totaling 26-30 neurons that generate the pyloric (food filtering, ~1 Hz) and gastric mill (food chewing, ~0.1 Hz) rhythms (Nusbaum and Beenhakker, 2002; Daur et al., 2016) (see Fig. 1). Multiple versions of each rhythm occur, with most STG neurons able to participate in both feeding networks, depending on the modulatory state (Dickinson et al., 1990; Weimann et al., 1991; Beenhakker et al., 2004; Bucher et al., 2006). Furthermore, neuromodulatory input-elicited neuronal switching is well established in the STNS (Hooper and Moulins, 1990; Meyrand et al., 1994).

In *C. borealis*, modulatory commissural neuron 5 (MCN5) elicits a novel rhythm in which the pyloric-only lateral posterior gastric (LPG) neuron switches participation to dual pyloric/gastric mill bursting (Norris et al., 1996; Blitz et al., 2019). During MCN5 activation, slower, long-duration gastric mill-timed bursts are superimposed on the faster pyloric-timed LPG bursting, despite strong electrical coupling to the pyloric pacemaker neurons (Blitz et al., 2019). Here, we examined whether electrical and/or chemical synaptic input is necessary for LPG to switch between single- and dual-network activity. We found that: (1) a both bath-applied and neuronally released neuropeptide elicits neuronal switching via modulation of intrinsic properties; and (2) electrical synaptic input works in concert with intrinsic properties to generate dual-frequency activity.

Materials and Methods

Animals. Adult male *C. borealis* crabs were obtained from the Fresh Lobster Company and maintained in artificial seawater at 10°C-12°C until used for experiments. Crabs were dissected to isolate the STNS (Gutierrez and Grashow, 2009; Blitz et al., 2019). Briefly, crabs were cold anesthetized by packing in ice for 35-50 min before dissection. The foregut was removed from the animal during gross dissection, bisected, and pinned flat in a Sylgard 170-lined dish (Thermo Fisher Scientific). During fine dissection, the STNS was carefully removed and pinned in a Sylgard 184-lined Petri dish (Thermo Fisher Scientific). For all parts of the dissection, the preparation was kept in chilled (4°C) *C. borealis* physiological saline.

Solutions. C. borealis physiological saline was composed of the following (in mM): 440 NaCl, 26 $MgCl_2$, 13 $CaCl_2$, 11 KCl, 10 Trizma base, 5 maleic acid, pH 7.4-7.6. Squid internal electrode solution contained the following (in mM): 10 $MgCl_2$, 400 potassium D-gluconic acid, 10 HEPES, 15 $NaSO_4$, 20 NaCl, pH 7.45 (Hooper et al., 2015). Gly^1-SIFamide (GYRKPPFNG-SIFamide, custom peptide synthesis: Genscript) (Huybrechts et al., 2003; Yasuda et al., 2004; Dickinson et al., 2008; Blitz et al., 2019) was dissolved in optima water (Thermo Fisher Scientific) at 10^{-2} M and aliquots stored at −20°C until needed. Gly^1-SIFamide aliquots were diluted in physiological saline to a final concentration of 5×10^{-6} M. PTX powder (Sigma Aldrich) was added directly to physiological saline at a final concentration of 10^{-5} M and

vigorously stirred for at least 45 min before use. For some experiments, Gly^1-SIFamide aliquots were added directly to PTX in physiological saline (10^{-5} M) at a final concentration of 5×10^{-6} M.

Electrophysiology. All preparations were continuously superfused with chilled *C. borealis* physiological saline (8°C-10°C), or chilled saline containing Gly^1-SIFamide and/or PTX as indicated. All solution changes were performed using a switching manifold for uninterrupted superfusion of the preparation. Using a model 1700 A-M Systems Amplifier, extracellular activity in nerves was recorded using custom-made stainless-steel pin electrodes, with one wire placed in Vaseline wells that were built around each nerve and one wire as reference outside the well. Stomatogastric ganglion (STG) somata were exposed by removing the thin layer of tissue across the ganglion and observed with light transmitted through a dark-field condenser (MBL-12 010 Nikon Instruments). Intracellular recordings of STG somata were obtained via sharp-tip glass microelectrodes (18-30 MΩ) filled with 0.6 M potassium acetate and 20 mM potassium chloride. For experiments involving intracellular LPG or MCN5 recordings, microelectrodes were filled with squid internal solution (20-40 MΩ) (see Solutions), which better maintains neuron properties over time (Hooper et al., 2015). All intracellular recordings were collected using AxoClamp 900A amplifiers in current-clamp mode (Molecular Devices). All experiments, excluding those with intracellular MCN5 recordings, were performed in the isolated STNS following transection of both inferior and superior oesophageal nerves (*ion* and *son*, respectively). For intracellular MCN5 recording experiments, the ipsilateral *ion* was not transected to retain the MCN5 projection to the STG. STG neurons were identified based on their nerve projection patterns and interactions with other STG neurons. All electrophysiological recordings were collected using acquisition hardware (Micro1401; Cambridge Electronic Design) and software (Spike2; ~5 kHz sampling rate, Cambridge Electronic Design) and laboratory computer (Dell).

Individual neurons, or subsets of neurons as indicated, were hyperpolarized to eliminate spike-mediated and graded transmitter release. Manipulated neurons included the pyloric neuron lateral pyloric (LP) and gastric mill neurons inferior cardiac (IC), dorsal gastric (DG), lateral gastric (LG), and medial gastric (MG). All intranetwork chemical synapses within the STG are inhibitory and mediated by either glutamate or acetylcholine (Marder and Bucher, 2007). The hyperpolarizing current injection amplitude (−2 to −4 nA; 200 s) was sufficient to decrease the voltage oscillation amplitude, indicating that the membrane potential was approaching reversal potential for inhibitory input and therefore below transmitter release threshold. Additionally, to eliminate rhythmic pyloric input the two pyloric dilator (PD) neurons were simultaneously hyperpolarized (−4 to −6 nA) for 200 s, except when the hyperpolarization was maintained for the duration of PTX:Gly^1-SIFamide applications to allow sufficient time to test the voltage dependence of LPG oscillations. Because of electrical coupling between anterior burster (AB) and the two PD neurons, hyperpolarization of the PD neurons hyperpolarizes AB, the main pacemaker in control conditions, and thus eliminates the pyloric rhythm (Bartos et al., 1999; Blitz et al., 2008).

To determine whether LPG bursting was voltage-dependent, we injected hyperpolarizing and depolarizing current into LPG (± 0.5, 1, 1.5, 2 nA) until at least 5 cycles occurred (a cycle is the time from the first spike in a LPG burst to the first spike in the next LPG burst), or 200 s passed without any cycles (<2 LPG bursts) taking place. These experiments were conducted during Gly^1-SIFamide in PTX with both PD neurons hyperpolarized to eliminate rhythmic pyloric electrical coupling input (PTX:PD_{hype}:Gly^1-SIFamide application).

MCN5 identification and stimulation. MCN5 was stimulated via intracellular current injection, or extracellular *ion* stimulation. The MCN5 soma was identified by correlating its spike activity with spikes in the *ion*, and by its effects on STG neurons (Norris et al., 1996; Blitz et al., 2019). There are only two neurons that project from the CoG to the STG via the *ion*: MCN5 and modulatory commissural neuron 1 (MCN1) (Coleman and Nusbaum, 1994; Bartos and Nusbaum, 1997). MCN1 and MCN5 have distinct effects, including opposite actions on several STG neurons (Coleman and Nusbaum, 1994; Norris et al., 1996; Bartos and Nusbaum, 1997; Blitz et al., 2019). For extracellular MCN5 stimulation, the *ion* was stimulated at 30 Hz (3-6 V; Grass S88 stimulator and Grass SIU5 stimulus isolation unit; Grass Instruments) when MCN5 activation threshold was lower than that of MCN1, or following photoinactivation of the MCN1 axon in the stomatogastric nerve (*stn*) near the entrance to the STG ($MCN1_{STG}$; see below) to eliminate MCN1 effects on STG neurons (Blitz et al., 2019).

Photoinactivation. Photoinactivation is used to selectively eliminate neuron activity from a network without influencing electrically coupled neurons (Miller and Selverston, 1979; Marder and Eisen, 1984). The LP neuron or $MCN1_{STG}$ was impaled with a sharp microelectrode (25-40 MΩ) that was tip-filled with AlexaFluor-568 hydrazide (10 mM in 200 mM KCl; Thermo Fisher Scientific) and backfilled with 0.6 M potassium acetate plus 20 mM potassium chloride. $MCN1_{STG}$ was identified based on the presence of 1:1 action potentials in $MCN1_{STG}$ during low-frequency (3 Hz) *ion* stimulation at MCN1 activation threshold, IPSPs from the LG neuron, and corresponding electrical EPSPs (eEPSPs) in LG (Coleman and Nusbaum, 1994; Coleman et al., 1995). Hyperpolarizing current (−5 nA) was injected into LP or LPG (~30 min) to fill the soma and neurites with the negatively charged Alexa-568 dye or to fill ~200-400 μm of the $MCN1_{STG}$ axon before its entrance into the STG (−5 nA, ~5 min). The STG or *stn* near its entrance to the STG was then illuminated for 3-7 min using a Texas red filter set (560 ± 40 nm wavelength; Leica Microsystems). Complete photoinactivation of LP or LPG was confirmed when the membrane potential reached 0 mV, and LP action potentials were absent from a lateral ventricular nerve (*lvn*) recording, or action potentials of the one photoinactivated LPG were absent from the lateral posterior gastric nerve (*lpgn)* (Miller and Selverston, 1979). Photoinactivation of $MCN1_{STG}$ was confirmed when the membrane potential reached 0 mV and there were no longer MCN1-elicited eEPSPs in LG during *ion* stimulations.

Data analysis. All analyses were conducted after MCN5 or Gly^1-SIFamide actions had reached a steady state. LP activity, including number of spikes per pyloric-timed burst and firing frequency ([number of spikes per burst − 1]/burst duration), was quantified across a 130-300 s window during sustained MCN5 stimulation or Gly^1-SIFamide application. To test whether MCN5 uses glutamate to inhibit LP, we measured LP number of spikes per burst, firing frequency, and the most depolarized peak membrane potential, excluding action potentials, during rhythmic MCN5 stimulation (5 s duration, 30 Hz intraburst frequency, 0.1 Hz interburst frequency). LP parameters were measured across 5 s blocks of alternating MCN5 stimulation off and on. Data from 10 blocks per condition (10 off, 10 on) per experiment were averaged during saline and PTX application (10^{-5} M). In PTX, LP bursts were defined based on inhibition from PD neurons, as these neurons use cholinergic transmission to inhibit the LP neuron, which is not blocked by PTX (Marder and Eisen, 1984).

LPG burst identification and analysis. The LPG interspike interval (ISI) distribution was used to identify LPG pyloric- and gastric mill-timed bursts. First, a histogram of LPG ISIs across an entire MCN5 stimulation or Gly^1-SIFamide application was generated and the two largest peaks were identified. The first of these peaks (within ~0-0.5 s) included intraburst intervals (interval between spikes during a burst), and the second peak (~0.5-2 s) included interburst intervals (interval between spikes between bursts). We calculated the mean ISI between these two peaks and used this value as a cutoff, such that ISIs above the cutoff indicated the end of one and beginning of another burst. A cutoff ISI was determined in this manner for each preparation and was used to detect both pyloric and gastric mill-timed bursts for each experimental manipulation. The ISI cutoff value was initially calculated in Excel and then using a custom-written MATLAB (MathWorks) function. To select only gastric mill-timed LPG bursts from all LPG bursts identified with the ISI cutoff, we used a custom-written Spike2 script, which identifies LPG bursts with a duration greater than one pyloric cycle period (from PD neuron burst onset to the subsequent PD neuron burst onset; ~1 s). Throughout the study, the number of these LPG gastric mill-timed bursts was quantified, as well as the LPG gastric mill-timed cycle period (duration between the first action potentials of two consecutive LPG gastric mill-timed bursts), burst duration (duration from the first to the last action potential in an LPG gastric mill-timed burst), and duty cycle (burst duration/cycle period) during MCN5 stimulation and Gly^1-SIFamide application.

To compare LPG bursts when isolated from both networks (10^{-5} M PTX:PD_{hype}) to pyloric- and gastric mill-timed bursts in network-intact conditions, we quantified LPG burst parameters across 5 LPG gastric mill (slow) cycles, including all the pyloric-timed cycles within that timeframe in control, and across 5 cycles of isolated LPG bursts. In two preparations in which MCN5 was stimulated, we were unable to analyze extracellular LPG activity and thus analyzed LPG activity from an intracellular recording. In a subset of the PTX:PD_{hype}:Gly^1-SIFamide application experiments, we recorded intracellularly from LPG and used multiple depolarizing and hyperpolarizing current injections to assess any voltage dependence of LPG bursting. In these experiments, we used action potentials from the intracellular LPG and measured the cycle period and duty cycle across 5 LPG slow cycles occurring at baseline and during the current injections used to shift the LPG voltage. We used ISI cutoff values (see above) to detect LPG bursts; however, the ISI value was adjusted when spikes that were visually part of an LPG burst were not included with the ISI value (i.e., spikes that occurred at the end of a burst before the membrane potential returned to the trough potential). Additionally, detected bursts that were shorter than an average pyloric cycle (1 s) were excluded from analysis (only necessary in 1 of 6 experiments). LPG activity was categorized as "tonic" when the ISI cutoff value detected no interburst intervals and therefore no bursts, for the duration of the current injection, and as "off" when there were no action potential bursts.

Spectral analysis. We used spectral analysis to quantify the degree to which LPG participates in the pyloric and gastric mill rhythms (Bucher et al., 2006; Rehm et al., 2008). All spectral analysis was conducted on LPG activity recorded extracellularly from the *lpgn*, which includes activity of the two LPG neurons, which were always coactive. As in Bucher et al. (2006), we excluded LPG spikes that occurred within 0.02 s of each other, which eliminates fast frequencies due to spikes of the two LPG neurons occurring in close proximity. To calculate the LPG power spectrum, we measured LPG instantaneous spike frequency (IF = 1/ISI) between each spike and all other spikes across each analysis window and plotted these values on a histogram to distinguish between gastric mill (0.05-0.19 Hz) and pyloric (0.2-4.0 Hz) burst frequencies (see Fig. 2*Aii*,*Bii*, blue and red regions, respectively). These windows exclude very low IFs (<0.05 Hz) occurring between spike pairs across multiple bursts, and high IFs occurring between nearby spikes within a burst (>4.0 Hz). The regions for gastric mill and pyloric activity were based on Bucher et al. (2006) and the observed gastric mill-timed cycle periods of LPG bursting in preliminary Gly^1-SIFamide application experiments. The counts of LPG gastric mill- and pyloric-timed IFs within these two regions were summed and then normalized to the total IF count between 0.05 and 4.00 Hz for each manipulation in each preparation. Normalized values were converted to a percentage to compare across preparations (see, e.g., Fig. 2*Aiv*,*Biv*). Pyloric and gastric mill percentages add to 100%; therefore, the amount of increase in one is the amount of decrease in the other, and statistical results for pyloric and gastric mill activity yield the same values. Thus, only LPG gastric mill percentages were analyzed statistically and reported in the text.

Software and statistical analysis. Raw data were analyzed using scripts/functions written in Spike2 or MATLAB. ISI histograms were made in Excel (Microsoft) or MATLAB. Statistical analysis was performed with SigmaPlot (Systat). Final figures were made using CorelDraw (Corel). Graphs were plotted in SigmaPlot and imported into CorelDraw. Data were first analyzed for normality using a Shapiro–Wilk test to determine whether a parametric or nonparametric test was to be used on each data set. Paired *t* test, Student's *t* test, Mann–Whitney Rank Sum test, Friedman one-way ANOVA on ranks, Friedman one-way repeated-measures ANOVA on ranks, Kruskal–Wallis one-way ANOVA on ranks, one-way repeated-measures ANOVA, Wilcoxon Signed Rank test, and *post hoc* tests for multiple comparisons were used as indicated. Threshold for significance was $p < 0.05$. All data are presented as mean ± SE.

Code accessibility. Spike2 scripts and MATLAB functions used for analysis are available on request from D.M.B.

Results

The STG within the STNS receives modulatory input from the bilateral commissural ganglia (CoGs) and the oesophageal ganglion (Fig. 1*A*). The modulatory projection neuron MCN5 soma is located in the CoG (one copy in each CoG), with axonal projections to the STG via the *ion*, *on*, and *stn* (Fig. 1*A*). The pyloric (red) and gastric mill (blue) network neurons within the STG are connected by inhibitory chemical, and electrical synapses (Fig. 1*B*). Similar to synapses across vertebrate and other invertebrate nervous systems, those in the STG are highly modulated. Here we indicate synapses that have been identified in *C. borealis* under a variety of conditions, although there are likely additional synapses yet to be identified. Gray boxes represent cellular targets of MCN5 (Fig. 1*B*); however, its modulation of synaptic connections has not yet been studied. The pyloric network is constitutively active *in vivo* and *in vitro* (Marder and Bucher, 2007; Stein, 2009), whereas the gastric mill network requires activation of modulatory projection or sensory neurons (Beenhakker et al., 2004; Blitz et al., 2004, 2008; Stein, 2009; Hedrich et al., 2011). When the gastric mill network is activated, some pyloric neuron activity becomes time-locked to both rhythms (red/blue) (Fig. 1*B*). MCN5 has classical and modulatory actions on most STG neurons and receives both long-distance and local presynaptic feedback from network neurons AB and pyloric (PY) neurons, respectively (Norris et al., 1996; Blitz et al., 2019).

Tonic MCN5 stimulation (30 Hz) alters the activity of both STG networks (Norris et al., 1996; Blitz et al., 2019) (Fig. 2*Ai*). In particular, the pyloric rhythm increases in frequency, evident in the increased frequency of PD neuron (*pdn*) bursts (Fig. 2*Ai*) (Norris et al., 1996; Blitz et al., 2019). Furthermore, a gastric mill rhythm is activated, indicated by the activation of rhythmic DG (*dgn*) neuron activity (Fig. 2*Ai*) (Blitz et al., 2019). In addition, MCN5 decreases activity in the LP neuron (Fig. 2*Ai*), and switches LPG neuron (*lpgn*) participation from pyloric only (Fig. 2*Ai*, left) to dual pyloric (black arrows) and gastric mill (white arrows) network bursting (Fig. 2*Ai*, right) (Norris et al., 1996; Blitz et al., 2019). We refer to this LPG switch to dual pyloric (fast)/gastric mill (slow) bursting as dual-network activity.

MCN5 releases a peptide cotransmitter, Gly^1-SIFamide (Blitz et al., 2019). Bath application of Gly^1-SIFamide (5×10^{-6} M) partially mimics neuronal release from MCN5 (Blitz et al., 2019) (Fig. 2*Bi*). Similar to tonic MCN5 stimulation, Gly^1-SIFamide application elicits an increase in pyloric frequency and activates a gastric mill rhythm (Blitz et al., 2019) (Fig. 2*Bi*, pyloric: *pdn*, gastric mill: *dgn*). In both MCN5 and Gly^1-SIFamide rhythms, there is variability in DG coordination with other gastric mill neurons (Blitz et al., 2019). However, a key distinction between MCN5 and Gly^1-SIFamide is in the LPG neuron response (Fig. 2*Ai*, *Bi*, *lpgn*). In control saline conditions, LPG is active only in pyloric time and coincident with PD neuron activity because of electrical coupling among the pyloric pacemaker neurons, AB, PD, and LPG (Marder and Eisen, 1984; Shruti et al., 2014) (Fig. 2*Ai*,*Bi*, left). During Gly^1-SIFamide (5×10^{-6} M) application, LPG continues to generate pyloric-timed bursts (*lpgn,* black arrows), as well as periodic, longer-duration bursts in which LPG activity extends beyond a single PD burst (*lpgn,* gray arrows), but does not persist for multiple pyloric cycles (Blitz et al., 2019) (Fig. 2*Bi*, right). These gastric mill-timed "envelopes" of extended bursting are in contrast to the gastric mill-timed LPG bursts during MCN5 stimulation, which persist for multiple pyloric cycles without interruption (Blitz et al., 2019) (Fig. 2*Ai*, white arrows).

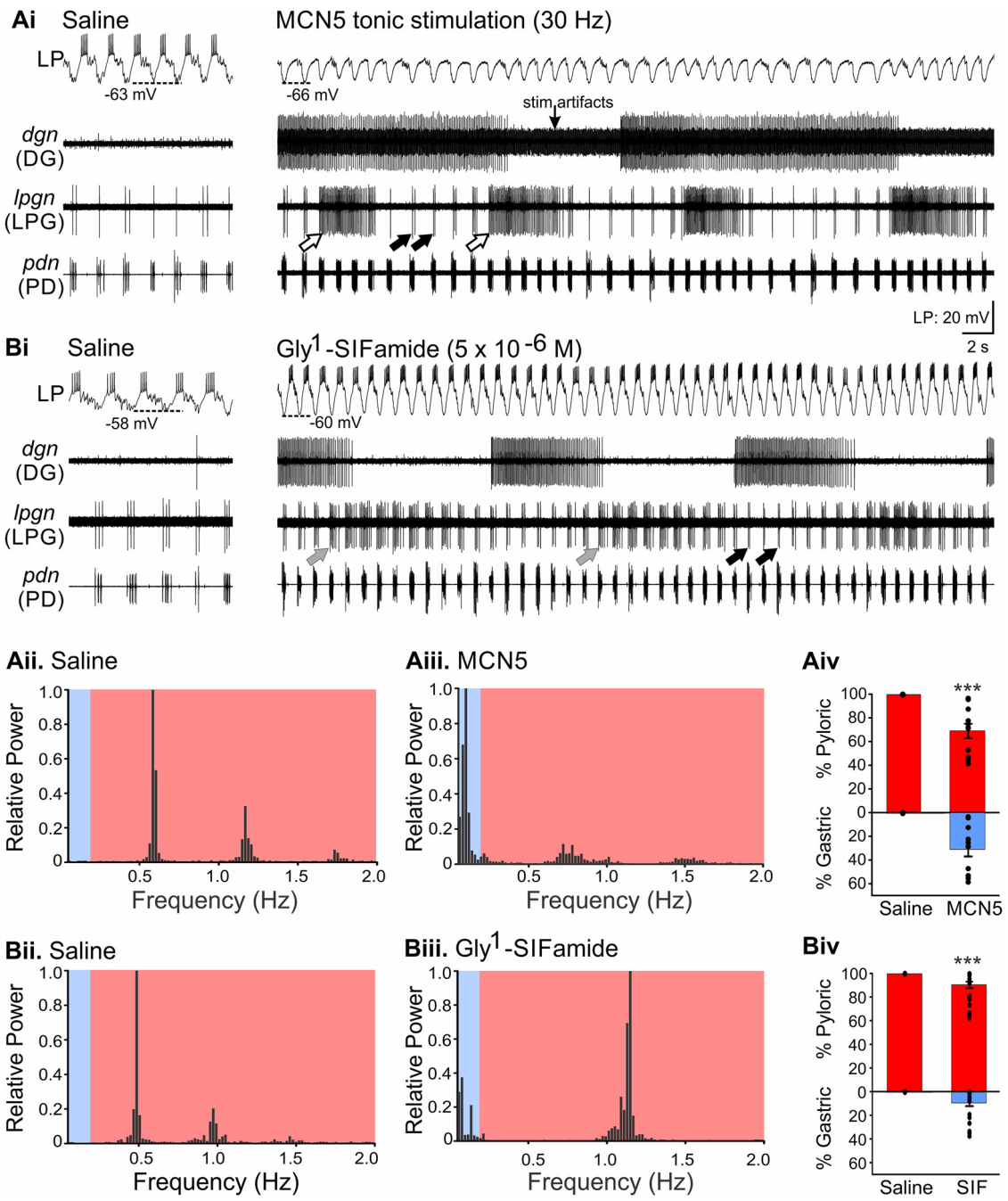

Figure 2. The MCN5 transmitter Gly^1-SIFamide does not entirely mimic the effects of MCN5 stimulation. ***Ai***, Left, In the control condition before MCN5 stimulation, the pyloric rhythm was active, evident in rhythmic bursting in the pyloric pacemaker neurons PD (*pdn*) and LPG (*lpgn*), and the LP neuron. Gastric mill neuron DG (*dgn*) was silent. Right, During tonic MCN5 stimulation (30 Hz), the pyloric rhythm was enhanced, evident by stronger, faster PD neuron bursting, and a gastric mill rhythm was activated, evident in the DG neuron bursting (*dgn*). Additionally, the LP neuron was inhibited, and the LPG neuron switched to dual pyloric- (black arrows) and gastric mill- (white arrows) timed bursting. ***Bi***, Left, Again, in control conditions, the pyloric rhythm was weakly active (PD, LPG, LP) and the gastric mill rhythm was not active (DG, *dgn*). Right, Bath application of Gly^1-SIFamide (5×10^{-6} M) strengthened LP neuron activity, activated DG, and increased the pyloric frequency (*pdn*). LPG (*lpgn*) did not switch to dual bursting; however, LPG exhibited periodic extensions of burst duration (gray arrows) for several pyloric cycles that coordinated with the gastric mill rhythm. ***Aii***, To quantify the pyloric- versus gastric mill-timed activity, the relative power across a range of instantaneous frequencies (IF; see Materials and Methods) was plotted. Blue area on the graph represents the gastric mill interburst frequencies (0.05-0.2 Hz). Red area represents the pyloric interburst frequencies (0.2-4.0 Hz). In saline, the spectral analysis indicates almost entirely pyloric-timed activity. For illustrative purposes, histogram plots are truncated at 2.0 Hz. ***Aiii***, During MCN5 stimulation, LPG dual-network activity is evident as peaks of relative power occurring within gastric mill (blue region) and pyloric (red region) frequencies in the relative power histogram. The total power from 0.05 to 4.0 Hz was summed across such a histogram for each condition, in each experiment, and the gastric mill and pyloric components calculated as a percentage of the total. ***Aiv***, The average percent pyloric activity across experiments is plotted in the upper portion, and average percent gastric mill activity plotted in the lower portion of the graph for illustrative purposes. Across experiments, a larger percentage of LPG activity was gastric mill-timed (blue box) during MCN5 stimulation compared with saline. Dots represent individual experiments, with a pyloric and a gastric mill value for each experiment which add to 100%. In control, the values were very close to 100% and 0% for pyloric- and gastric mill-timed activity, respectively; thus, dots overlap. ***Bii-Biii***, Relative power is plotted for saline, followed by Gly^1-SIFamide application. ***Biv***, The average percent pyloric and gastric mill activity across experiments during saline versus Gly^1-SIFamide application is plotted. For ease of comparison, each relative power histogram was normalized to the largest peak within the *x* range shown. ***A***, ***B***, From the same preparation. MCN5 ($n = 11$), Gly^1-SIFamide ($n = 23$). $^{***}p < 0.001$. ***Aiv***, Paired *t* test; ***Biv***, Signed Rank Test.

In order to extend previous results (Blitz et al., 2019) and quantitatively compare LPG activity during MCN5 stimulation and Gly^1-SIFamide application, we developed criteria to identify gastric mill-timed bursts. Specifically, LPG bursts were identified based on a minimum interburst ISI, and a minimum burst duration that was longer than one pyloric cycle (see Materials and Methods). Using these criteria, four LPG slow bursts occurred during the example MCN5 stimulation (tonic 30 Hz; Fig. 2*Ai*, right), whereas zero LPG bursts met the criteria for a slow burst in an example Gly^1-SIFamide application (Fig. 2*Bi*, right). Across preparations, LPG generated more slow bursts during MCN5 stimulation versus Gly^1-SIFamide application within 200 s analysis windows (MCN5: 13 ± 2.1, $n = 11$; Gly^1-SIFamide: 4.7 ± 1.2, $n = 27$; $U = 45.5$, $p < 0.001$, Mann–Whitney Rank Sum Test).

Although the number of LPG slow bursts is useful to determine LPG participation in the gastric mill rhythm, it does not provide a measure of LPG dual-network activity. Thus, we used spectral analysis to quantify LPG dual-network (pyloric plus gastric mill) activity (Bucher et al., 2006; Rehm et al., 2008) (see Materials and Methods). Spectral analysis quantifies the extent of spiking activity across frequencies (Bucher et al., 2006; Rehm et al., 2008). For this analysis, we generated a histogram of the relative power of LPG activity across a range that included interburst spike frequencies (0.05-4 Hz) but not intraburst spike frequencies (Fig. 2*Aii*,*Aiii*,*Bii*,*Biii*). From the histogram, the relative power was summed across interburst spike frequencies corresponding to gastric mill timing (0.05-0.19 Hz; Fig. 2*Aii*,*Aiii*,*Bii*,*Biii*, blue area) and pyloric timing (0.2-4.0 Hz; Fig. 2*Aii*,*Aiii*,*Bii*,*Biii*, red area, *x* axis truncated at 2.0 Hz in the examples for viewing ease). These values were normalized to the total sum of relative power across gastric mill- and pyloric-timed interburst spike frequencies, converted to a percentage, and averaged across experiments (Fig. 2*Aiv*,*Biv*; see Materials and Methods). Gastric mill percent values are graphically represented below the pyloric percent values with gastric mill plus pyloric adding to 100%. In saline in the example shown (Fig. 2*Aii*), almost all peaks in the histogram occurred within the pyloric region of the histogram; and the percent of LPG activity corresponding to gastric mill and pyloric timing was 0.3% and 99.7%, respectively. During tonic (30 Hz) MCN5 stimulation, LPG was bursting in both pyloric and gastric mill time, evident as peaks of relative power in both gastric mill and pyloric frequencies (Fig. 2*Aiii*). The overall LPG gastric mill and pyloric percentages were 55.5% and 44.5%, respectively, in this preparation. Across experiments, tonic MCN5 stimulation switched LPG to 31.0 ± 6.1% gastric mill-timed activity versus 0.3 ± 0.1% in control (Fig. 2*Aiv*; $n = 11$; $t_{(10)} = -5.04$, $p = 5.1 \times 10^{-4}$, paired *t* test). During Gly^1-SIFamide application, LPG generated envelopes of extended bursting but produced few slow bursts (as described above) (Fig. 2*Bi*). In the example shown, Gly^1-SIFamide also caused a shift from the spectral power being almost entirely within pyloric burst frequencies (pyloric sum: 0.4%; gastric sum: 99.6%) in saline (Fig. 2*Bii*) to both pyloric (red region) and gastric (blue region) peaks, although it appeared to be a smaller amount of gastric activity (Fig. 2*Biii*) compared with during MCN5 stimulation (Fig. 2*Aiii*). Across experiments, bath-applied Gly^1-SIFamide elicited 9.6 ± 2.7% gastric mill-timed activity compared with 0.3 ± 0.04% in control (Fig. 2*Biv*; $n = 23$; *Z* statistic = 4.02, $p < 0.001$, Wilcoxon Signed Rank Test). Spectral analysis thus enables us to quantify the extent of single- versus dual-network activity of LPG with a single value (% gastric mill-timed activity; Fig. 2*Aiv*,*Biv*). Using this measure, MCN5 elicited greater dual-network activity in LPG compared with Gly^1-SIFamide bath application (MCN5: 31.0 ± 6.1%, $n = 11$; Gly^1-SIFamide: 9.6 ± 2.7%, $n = 27$; $U = 53.0$, $p = 0.002$, Mann–Whitney Rank Sum Test). Thus, quantification of LPG slow burst number and the percent gastric mill-timed activity aligns with the previous qualitative assessment (Blitz et al., 2019), that Gly^1-SIFamide does not entirely mimic the MCN5-elicited LPG switch from single- to dual-network activity.

Gly^1-SIFamide and LP photoinactivation to model MCN5 stimulation

To determine why Gly^1-SIFamide did not entirely mimic the MCN5 actions on LPG, we considered the well-described circuitry of the pyloric and gastric mill networks, as well as other Gly^1-SIFamide effects. LPG receives two known inputs from STG neurons: (1) feedback inhibition from the LP neuron and (2) electrical synaptic input from the pyloric pacemaker ensemble (Marder and Eisen, 1984; Shruti et al., 2014) (Fig. 1*B*). Although additional inputs to LPG are likely to be effective in the Gly^1-SIFamide/MCN5 modulatory state, here we considered the two known network inputs to LPG. Similar to MCN5 stimulation, bath application of Gly^1-SIFamide (5×10^{-6} M) elicits an increase in pyloric cycle period (Blitz et al., 2019). Thus, the influence of the pyloric pacemaker ensemble via electrical coupling to LPG is likely similar in the two conditions. However, unlike the MCN5 direct inhibition of LP (Norris et al., 1996) (Fig. 2*Ai*), Gly^1-SIFamide application excites LP (Blitz et al., 2019) (Fig. 2*Bi*). The previous characterization of MCN5 inhibition of LP used brief (10 s) MCN5 stimulation. To better compare the effects of MCN5 and its bath-applied transmitter on LP, we measured LP activity during sustained tonic MCN5 stimulation and Gly^1-SIFamide application. We found that LP activity during Gly^1-SIFamide application was stronger in terms of number of spikes per burst and firing rate compared with during MCN5 stimulation (LP no. of spikes/burst: MCN5: 3.51 ± 0.70, $n = 11$; Gly^1-SIFamide: 7.14 ± 0.61, $n = 27$; $t_{(36)} = -3.42$, $p = 0.002$, Student's *t* test; LP spike frequency: MCN5: 11.46 ± 1.76 Hz, $n = 11$; Gly^1-SIFamide: 18.31 ± 1.45 Hz, $n = 27$; $t_{(36)} = -2.70$, $p = 0.011$, Student's *t* test). The different effects of Gly^1-SIFamide and MCN5 stimulation on LP suggested the possibility that MCN5 uses a cotransmitter to inhibit LP activity.

A common inhibitory neurotransmitter in the STNS is glutamate (Marder and Eisen, 1984; Cleland and Selverston, 1995); thus, we tested whether MCN5 uses glutamate to inhibit LP. Rhythmic MCN5 stimulation (intraburst frequency: 30 Hz; interburst frequency: 0.1 Hz, burst duration: 5 s) was used to assess MCN5 inhibition of LP. In control saline conditions, LP was bursting in pyloric time. Each MCN5 stimulation decreased the number of LP spikes per burst (saline: 6.0 ± 0.9; MCN5: 2.3 ± 0.7, $n = 6$; $t_{(5)} = 3.8$, $p = 0.01$, paired *t* test), decreased LP firing frequency (saline: 15.5 ± 2.1 Hz; MCN5: 7.3 ± 2.7 Hz, $n = 6$; *Z* statistic = −2.2, $p = 0.031$, Wilcoxon Signed Rank Test), and caused a hyperpolarization of the LP membrane potential at the peak of its oscillations (saline: −40.6 ± 2.0 mV; MCN5: −49.2 ± 2.8 mV, $n = 6$; $t_{(5)} = 4.40$, $p = 0.007$, paired *t* test) (Fig. 3, left). Also, LPG generated a gastric mill-timed burst during each MCN5 stimulation (Fig. 3, *lpgn*). To test whether MCN5 inhibition of LP was mediated by glutamate, we used PTX (10^{-5} M), which blocks inhibitory glutamatergic transmission in the STNS (Bidaut, 1980; Marder and Eisen, 1984; Cleland and Selverston, 1995). To verify that PTX effectively blocked glutamatergic inhibition, we used LP and PY neuron activity. These neurons are electrically coupled and reciprocally inhibit each other via glutamatergic synapses (Graubard and Hartline, 1987; Mamiya et al., 2003). Under baseline conditions, the chemical inhibition

dominates and LP and PY activity is largely nonoverlapping (Mamiya et al., 2003) (Fig. 3, left expanded *lvn*). Blocking glutamatergic inhibition with PTX eliminates LP and PY chemical inhibition of each other, leaving only electrical coupling, such that their activity is coincident (Bidaut, 1980). Thus, overlapping LP and PY activity was used to verify the efficacy of PTX (Fig. 3, right expanded *lvn*). In PTX, LP peak voltage was less hyperpolarized, and its burst was extended because of the block of PY inhibition (Fig. 3, right). In this condition, MCN5 stimulation decreased LP spike number (PTX: 10.3 ± 0.7; MCN5: 6.2 ± 0.8, $n = 6$; $t_{(5)} = 5.44$, $p = 0.003$, paired t test), but not spike frequency (PTX: 11.5 ± 0.7 Hz; MCN5: 11.0 ± 0.7 Hz, $n = 6$; $t_{(5)} = 1.49$, $p = 0.197$, paired t test) or peak voltage (PTX: -35.2 ± 0.8 mV; MCN5: -35.6 ± 0.9 mV, $n = 6$; $t_{(5)} = 2.25$, $p = 0.074$, paired t test) (Fig. 3, right). In PTX, the decreased LP number of spikes per burst caused by MCN5 stimulation was likely because of PD neuron inhibition of LP, as the PD neurons are cholinergic, and their chemical inhibitory transmission is not blocked by PTX (Marder and Eisen, 1984). In PTX, the increased PD burst frequency during MCN5 stimulation truncated the LP burst duration (Fig. 3, right) (PTX: 0.8 ± 0.07 s; MCN5: 0.5 ± 0.07 s, $n = 6$; $t_{(5)} = 3.8$, $p = 0.013$, paired t test), resulting in fewer LP spikes per burst. However, the lack of a change in LP spike frequency and peak voltage in response to MCN5 stimulation indicates that the direct MCN5 inhibition of LP was blocked by PTX. Thus, MCN5 appears to use glutamate as a cotransmitter to inhibit LP, whereas its modulation of LPG occurs via Gly^1-SIFamide (Fig. 3) (Blitz et al., 2019).

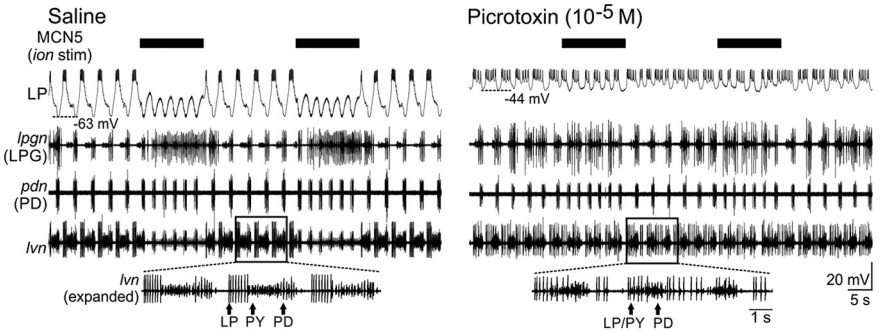

Figure 3. MCN5 uses its cotransmitter glutamate to inhibit LP. Left, Rhythmic MCN5 stimulation (30 Hz, 5 s; black bars) inhibited LP, evident by the elimination of spiking and a more hyperpolarized peak membrane potential. During each MCN5 stimulation, there was a slow burst elicited in LPG (*lpgn*). The expanded region of the extracellular *lvn* recording highlights that the LP and PY neurons fired out of phase because of their reciprocal inhibition, which has a stronger effect than the electrical coupling between them. Right, In the presence of PTX (10^{-5} M), MCN5 stimulation increased the pyloric frequency and elicited slow bursts in LPG; however, it did not inhibit LP. Baseline LP activity is different in PTX because of the block of glutamatergic inhibition, including that from the AB and PY neurons (Bidaut, 1980; Marder and Eisen, 1984; Graubard and Hartline, 1987; Cleland and Selverston, 1995; Mamiya et al., 2003). The efficacy of PTX is evident in the expanded *lvn* trace in which LP and PY now overlap because glutamatergic inhibition between them is blocked, but their electrical coupling remains. LP still bursts in pyloric time because of the remaining inhibition from the cholinergic PD neuron. Left and right images are from the same preparation.

In contrast to the MCN5-elicited glutamatergic inhibition of LP, bath-applied Gly^1-SIFamide increased LP spikes per burst and firing rate, as discussed above and reported by Blitz et al. (2019). Consequently, it is unlikely that bath-applied Gly^1-SIFamide effects on LP mimic the actions of Gly^1-SIFamide released from MCN5. In addition to MCN5, there is another Gly^1-SIFamide-containing input projecting from each CoG to the STG (Blitz et al., 2019), and Gly^1-SIFamide excitation of LP more likely mimics the actions of this other unidentified Gly^1-SIFamide modulatory neuron.

Since LP inhibits LPG, we explored whether stronger LP activity during Gly^1-SIFamide application prevented LPG from generating gastric mill-timed (slow) bursts that occur during MCN5 stimulation. We first examined whether there was a relationship between LP activity and LPG slow bursting and found a negative correlation between the number of LPG slow bursts and LP spike frequency in Gly^1-SIFamide (Fig. 4*A*; $n = 26$; $r^2 = 0.39$, $p = 5.9 \times 10^{-4}$, Pearson correlation). Although average LP activity was lower during MCN5 stimulation compared with Gly^1-SIFamide, there was also a negative correlation between the number of LPG slow bursts and LP spike frequency during tonic MCN5 stimulation (Fig. 4*A*; $n = 11$, $r^2 = 0.36$, $p = 0.049$, Pearson correlation). In several preparations during Gly^1-SIFamide application, there were zero LPG slow bursts (Fig. 4*A*, filled circles along x axis), but no instances of zero LPG slow bursts during MCN5 stimulation (Fig. 4*A*, open circles). These data support stronger LP activity in Gly^1-SIFamide application as a cause of the lower LPG dual-network activity in Gly^1-SIFamide compared with during MCN5 stimulation.

To further explore whether LP activity was responsible for the difference in LPG activity between MCN5 and Gly^1-SIFamide application, we tested whether LP hyperpolarization during Gly^1-SIFamide application enabled LPG to switch to dual-network activity, similar to its response to MCN5 stimulation. In Gly^1-SIFamide (5×10^{-6} M), LP was active, and LPG generated bursts in pyloric time, with some bursts extending beyond the end of a PD burst (Fig. 4*B*, left traces, red boxes) (Blitz et al., 2019). However, when LP was hyperpolarized during Gly^1-SIFamide, LPG generated slow gastric mill-timed bursts (blue box) that alternated with multiple cycles of faster pyloric bursts (red boxes) (Fig. 4*B*, right). As above, the percentage of LPG gastric mill-timed activity calculated via spectral analysis differed between MCN5 stimulation and Gly^1-SIFamide application (SIF-LP ON), but was similar between MCN5 stimulation and Gly^1-SIFamide application with LP hyperpolarized (SIF-LP OFF) (Fig. 4*C*) (MCN5: $31.0 \pm 6.1\%$, $n = 11$; SIF-LP ON: $10.1 \pm 3.6\%$, $n = 15$; SIF-LP OFF: 28.4 ± 4.1 $n = 15$; $H_{(3)} = 20.93$, $p < 0.001$, Kruskal–Wallis one-way ANOVA on ranks; MCN5 vs SIF-LP ON: $p = 0.02$; MCN5 vs SIF-LP OFF: $p = 1.0$; SIF-LP ON vs SIF-LP OFF: $p = 0.025$, Dunn's method for pairwise comparisons). Although hyperpolarizing LP enabled LPG to switch to dual-network activity in Gly^1-SIFamide, it was possible that the current injection into LP was influencing other network neurons via electrical coupling (Fig. 1*B*) (Graubard and Hartline, 1987; Mamiya et al., 2003; Marder and Bucher, 2007). We thus moved to photoinactivation, which enables the permanent removal of a neuron without affecting electrically coupled neurons (Miller and Selverston, 1979; Marder and Eisen, 1984; Faumont et al., 2005) (see Materials and Methods). After photoinactivation ("Kill") of LP, LPG generated dual-network activity in Gly^1-SIFamide that was similar to that during Gly^1-SIFamide with LP hyperpolarized, and during tonic MCN5 stimulation (Fig. 4*C*; $H_{(3)} = 20.93$, $p < 0.001$, Kruskal–Wallis one-way ANOVA on ranks; SIF-LP Kill [$n = 39$] vs SIF-LP OFF [$n = 15$]: $p = 1.00$; SIF-LP Kill [$n = 39$] vs MCN5 [$n = 11$]: $p = 1.00$, Dunn's method for pairwise comparisons). These results indicate that Gly^1-

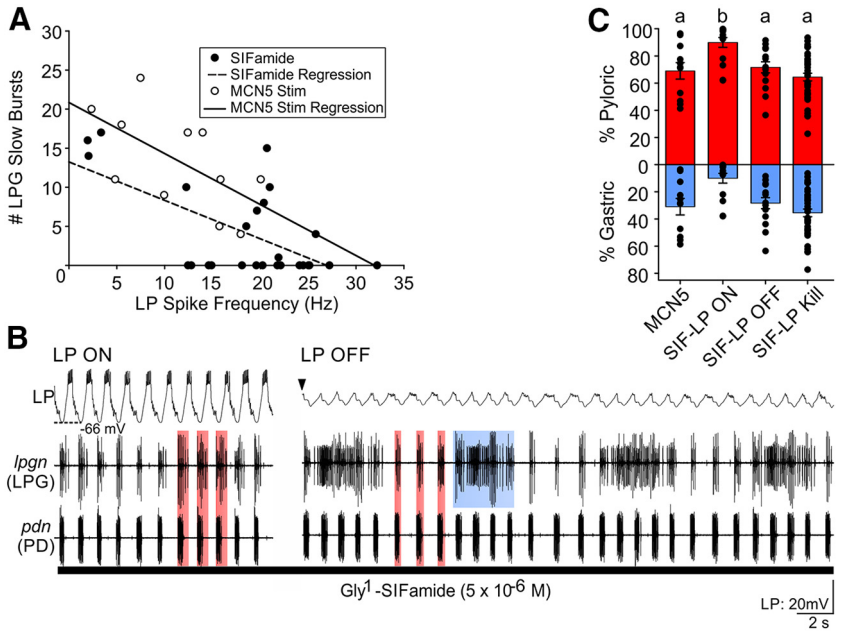

Figure 4. Gly[1]-SIFamide more closely mimics MCN5-elicited effects in the absence of LP. ***A***, A plot of the number of LPG slow bursts versus LP firing frequency indicates that during MCN5 stimulation (open circles) and Gly[1]-SIFamide application (filled circles), there is a greater number of LPG slow bursts with lower LP firing frequency. In several experiments, Gly[1]-SIFamide elicited 0 LPG slow bursts. Regression lines indicate the negative correlation between the number of LPG slow bursts and LP firing frequency for MCN5 (solid line) and Gly[1]-SIFamide (dashed line). MCN5: $n = 11$; Gly[1]-SIFamide: $n = 25$. ***B***, Left, With LP intact, LPG is primarily pyloric-timed in Gly[1]-SIFamide (5×10^{-6} M) with periodic bursts (*lpgn*) that extend beyond the end of the pyloric PD bursts (red boxes), but no slow gastric mill-timed bursts. Right, During the Gly[1]-SIFamide application, hyperpolarization of LP caused LPG bursting to switch to both pyloric- (red boxes) and gastric mill- (blue box) timed activity. Neurons were recorded with an unbalanced bridge, and the hyperpolarized trace is aligned for ease of visualization, not to represent an accurate membrane potential. ***C***, Across experiments, the average percent of LPG pyloric (red) and gastric mill (blue) activity was similar between MCN5 stimulation, Gly[1]-SIFamide with LP hyperpolarized (SIF-LP OFF) and Gly[1]-SIFamide with LP photoinactivated (SIF-LP Kill; see Materials and Methods). However, the LPG activity was less gastric mill-timed during Gly[1]-SIFamide application with LP active (SIF-LP ON). Dots represent individual experiments, with a pyloric and a gastric mill value for each experiment that add to 100%. MCN5 ($n = 11$), SIF-LP ON ($n = 15$), SIF-LP OFF ($n = 15$), and SIF-LP Kill ($n = 39$). Similar letters indicate no statistical difference. Different letters indicate significance. Kruskal–Wallis one-way ANOVA on ranks, Dunn's method for pairwise comparison.

SIFamide application with LP activity eliminated more closely mimics MCN5-elicited actions and enables us to examine mechanisms underlying LPG switching to dual-network activity. Therefore, for the remainder of this study, Gly[1]-SIFamide applications were performed with the LP neuron photoinactivated unless otherwise noted.

Gastric mill neuron input is not necessary for LPG to generate dual-network activity

Strengthening chemical synaptic input from network neurons to recruit a switching neuron into another network is the established mechanism for neuronal switching (Dickinson et al., 1990; Hooper and Moulins, 1990; Meyrand et al., 1994; Weimann and Marder, 1994). Therefore, we tested whether LPG required synaptic input from gastric mill neurons to switch to dual-network activity. There are nine neuron types that can participate in a gastric mill rhythm (Fig. 1*B*) (Weimann et al., 1991). In gastric mill rhythms elicited by modulatory inputs other than MCN5, the reciprocally inhibitory LG and interneuron 1 (Int1) neurons are the core rhythm generators (Coleman et al., 1995; White and Nusbaum, 2011). LG changes from silent to bursting on activation of a gastric mill rhythm, including the MCN5/Gly[1]-SIFamide gastric mill rhythm (Coleman et al., 1995; Beenhakker et al., 2004; White and Nusbaum, 2011; Blitz et al., 2019). In the absence of a gastric mill rhythm, Int1 is active in pyloric time because of rhythmic inhibition from the pyloric pacemakers (Fig. 1*B*) (Weimann et al., 1991; Bartos et al., 1999). During a gastric mill rhythm, however, its pyloric-timed activity is rhythmically inhibited in gastric mill time by LG (Coleman et al., 1995; Bartos and Nusbaum, 1997; White and Nusbaum, 2011). Using Int1 IPSPs in LG, we verified that Int1 is active with both the pyloric and gastric mill rhythm during Gly[1]-SIFamide application (Fig. 5*Ai*) ($n = 11/11$). Specifically, when Int1 is active, pyloric-timed IPSP barrages occurred between PD neuron bursts. They did not occur during LG gastric mill-timed bursts, when LG is inhibiting Int1 (Fig. 5*Ai*). This Int1 input to LG is responsible for the pyloric-timed subthreshold oscillations in the LG interburst during gastric mill rhythms (Coleman et al., 1995; Bartos et al., 1999) (Fig. 5*Bi*).

To determine whether LG and Int1 are necessary for LPG slow bursting, we eliminated LG activity with hyperpolarizing current injection, which also changed Int1 activity to pyloric only (Fig. 5*Aii*) ($n = 11/11$). In the example shown, IPSP barrages caused pyloric-timed depolarizations, as LG was hyperpolarized below the reversal potential for these synaptic events (Fig. 5*Aii*). During this LG hyperpolarization, LPG slow bursting continued during Gly[1]-SIFamide despite the absence of alternating LG/Int1 activity (Fig. 5*Bii*), indicating that LPG dual activity does not require gastric mill-timed input from these two neurons. Across experiments, LPG generated dual pyloric- (red bars) and gastric mill-timed (blue bars) bursting during Gly[1]-SIFamide application whether LG was active (SIF-ON-Pre) or hyperpolarized (SIF-OFF) (Fig. 5*Biii*).

In the MCN5/Gly[1]-SIFamide gastric mill rhythm, in addition to LG, the IC and DG neurons are most strongly activated in gastric mill time (Blitz et al., 2019). Thus, we examined whether these neurons are necessary to recruit LPG into the gastric mill network and generate dual-network activity. In the examples shown, each of these neurons was bursting in gastric mill time during Gly[1]-SIFamide (5×10^{-6} M) application (Fig. 5*Ci,Di,Ei*). We injected hyperpolarizing current in each neuron, individually (Fig. 5*Cii,Dii*) and simultaneously (Fig. 5*Eii*), to remove their activity during Gly[1]-SIFamide bath application. LPG continued to generate slower gastric mill-timed bursts and thus dual-network activity during hyperpolarization of the IC neuron (Fig. 5*Cii*), DG neuron (Fig. 5*Dii*), and LG, IC, DG neurons, simultaneously (Fig. 5*Eii*). Across preparations, LPG did not require gastric mill-timed IC (Fig. 5*Ciii*, $n = 19$) or DG (Fig. 5*Diii*, $n = 14$) activity, or LG/Int1/IC/DG combined activity (Fig. 5*Eiii*, $n = 15$) to generate dual-frequency bursting (red + blue bars). Although the MG neuron is electrically coupled to the LG neuron, and thus likely hyperpolarized along

with LG, we separately tested whether MG was necessary for the switch in LPG activity. We found that LPG generated dual-network activity in Gly[1]-SIFamide during MG hyperpolarization (Table 1, $n = 6$). Among the remaining gastric mill neurons, the VD neuron gastric mill activity is because of rhythmic inhibition from LG (Weimann and Marder, 1994); thus, VD was only active in pyloric time during hyperpolarization of LG (data not shown). As indicated above, this did not prevent dual activity in LPG. The AM neuron activity during Gly[1]-SIFamide application was variable. Specifically, AM exhibited gastric mill-timed bursting in 3 of 7 preparations and was silent or only sporadically active in the remaining (4 of 7) preparations, and thus was not examined further in this study. GM neurons are not excited by Gly[1]-SIFamide (Blitz et al., 2019), and were not examined in this study. Thus, LPG is not recruited into a second network via synaptic input from gastric mill neurons.

Quantifying the extent to which a neuron is participating in multiple rhythms is challenging (Bucher et al., 2006). Spectral analysis provides a way to compare the extent of dual activity across multiple preparations (Bucher et al., 2006); however, by collapsing the bursting activity into a single value for pyloric and gastric mill activity, details about the activity are lost. For example, during IC hyperpolarization, the LPG slow bursting appeared to occur at a faster frequency in the example shown, but changes in burst parameters cannot be assessed from the spectral analysis. Although there was gastric mill-timed activity with all hyperpolarizations, there were differences in the percent gastric mill activity between SIF-ON-Pre and SIF-OFF for all manipulations except DG hyperpolarization (Fig. 5*Biii, Ciii, Diii, Eiii*; Table 1), but some SIF-OFF percentages were not different from those after removal of hyperpolarization (Table 1: SIF-ON-Post). A decreased percent gastric mill activity suggests that other gastric mill neurons regulate LPG slow bursting, even if they are not necessary for it. However, our statistical analysis suggests there may be some rundown of the slow bursting during these ~20-45 min applications. Determining whether gastric mill neurons regulate LPG slow bursting in a quantitative manner will require additional experiments and different analyses. We did not pursue interactions between gastric mill neurons in this study, instead focusing on the continued presence of LPG gastric mill-timed bursting during hyperpolarization of other gastric mill neurons as evidence that they are not necessary for LPG dual-network activity to occur in Gly[1]-SIFamide.

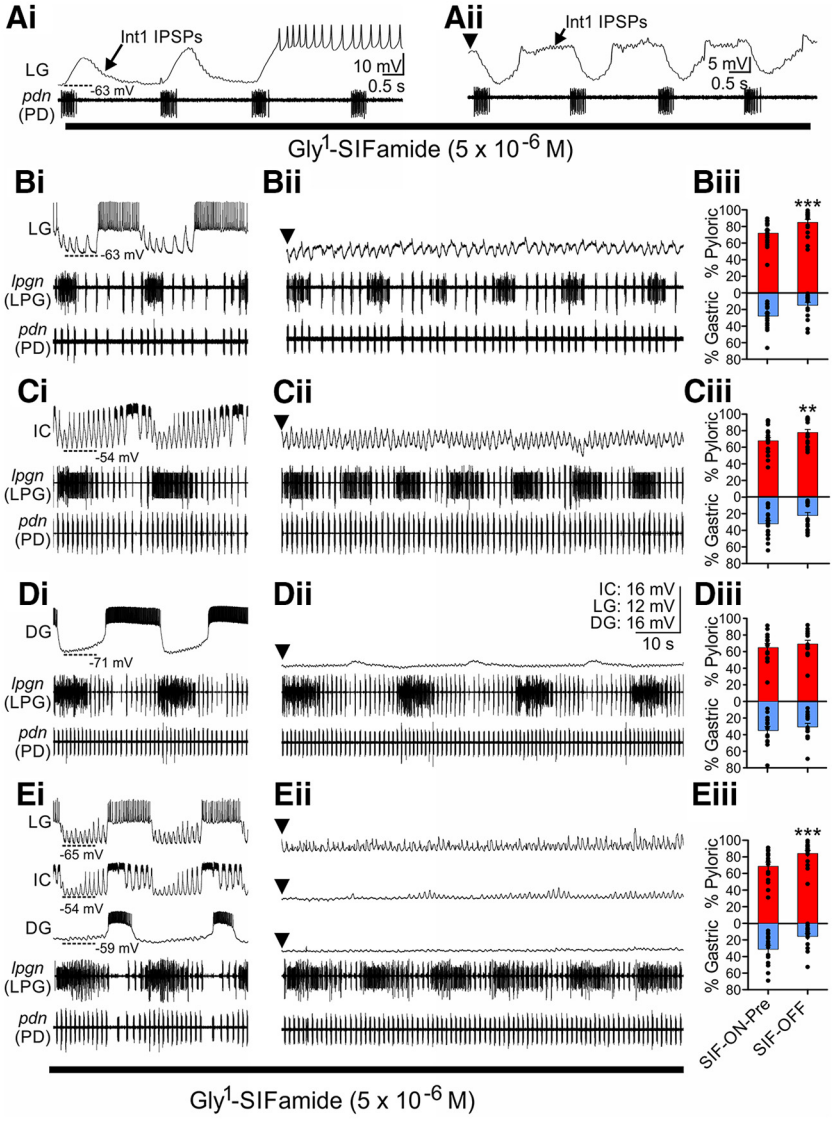

Figure 5. The LPG switch to dual bursting does not require activity from other gastric mill network neurons during Gly[1]-SIFamide bath application. ***Ai***, During Gly[1]-SIFamide application, there were rhythmic barrages of IPSPs in LG from the Int1 neuron (arrow). IPSPs were eliminated in time with each PD neuron burst and during the LG burst. ***Aii***, During LG hyperpolarization, Int1 IPSPs occurred in pyloric time but were depolarizing because of the LG membrane potential being hyperpolarized below their reversal potential. ***Bi-Ei***, Gly[1]-SIFamide application with LP photoinactivated elicited dual-network bursting in LPG (*lpgn*), gastric mill-timed activity in LG and DG, and both gastric mill and pyloric bursting in IC. ***Bii-Eii***, LPG continued to express dual bursting when LG (***Bii***), IC (***Cii***), DG (***Dii***), or LG, IC, and DG (***Eii***) activity was eliminated with hyperpolarizing current injection (downward-pointing arrowheads). During current injections, neurons were recorded with an unbalanced bridge, and hyperpolarized traces are aligned for ease of visualization, not to represent actual membrane potentials. The average percent pyloric and gastric mill activity is plotted during Gly[1]-SIFamide application before manipulation (SIF-ON-Pre) and during hyperpolarization (SIF-OFF) of LG (***Biii***), IC (***Ciii***), DG (***Diii***), and LG, IC, and DG (***Eiii***). There was a decrease in the amount of LPG gastric mill activity when LG, IC, and LG, IC, and DG were hyperpolarized. ***A***, ***B***, From the same experiment. ***C-E***, From separate experiments. ***B***, ***C***, ***E***, One-way repeated-measures ANOVA, Holm-Sidak *post hoc*. ***D***, Friedman repeated-measures ANOVA on ranks. $^{**}p < 0.01$; $^{***}p < 0.001$ (see Table 1).

Pyloric pacemaker activity is not required for LPG gastric mill-timed bursting

Despite LPG not requiring gastric mill input to generate dual-network activity, it is possible that pyloric network neurons contribute to LPG switching to dual-network activity. Pyloric network input to LPG includes inhibition from LP, which was photoinactivated in our experiments, and electrical coupling to the other pacemaker ensemble neurons, the two PD and single AB neurons (Fig. 1*B*) (Marder and Bucher, 2007). In control conditions, AB is the pacemaker, and its rhythmic activity drives

Table 1. Percent of LPG gastric mill-timed bursting with/without gastric mill network and pyloric pacemaker neuron activity

Neurons hyped	Mean ± SE					*p* value		
	Gly[1]-SIFamide							
	Pre[a]	OFF	Post	*F/H*	df	OFF vs ON-Pre	OFF vs ON-Post	ON-Pre vs ON-Post
LG ($n = 17$)	28.0 ± 3.6	15.0 ± 3.6	22.4 ± 3.9	35.5**	16,2	<0.001	<0.001	0.001
IC ($n = 19$)	31.2 ± 3.8	22.0 ± 3.7	26.1 ± 3.7	5.8**	18,2	0.005	0.14	0.13
DG ($n = 14$)	35.1 ± 4.8	30.8 ± 4.4	26.2 ± 4.2	14.3*	13,2	0.14	0.14	<0.001
LG/IC/DG ($n = 15$)	31.3 ± 4.9	15.8 ± 3.7	25.1 ± 3.4	14.3**	14,2	<0.001	0.007	0.04
MG ($n = 6$)	14.2 ± 2.8	12.6 ± 4.1	10.9 ± 3.6	3.3**	5,2			
PD/PD ($n = 9$)	28.8 ± 6.0	81.3 ± 2.6	28.2 ± 6.4	67.0**	8,2	<0.001	<0.001	0.91

[a]During Gly[1]-SIFamide application: Pre, before neuron(s) turned off; OFF, neuron(s) turned off; Post, after neuron(s) turned off; PD/PD, pyloric pacemaker neurons. *Post hoc* not performed when $p > 0.05$.
*χ^2 value (H), Friedman repeated-measures ANOVA on ranks, Tukey's *post hoc*.
**F value, one-way repeated-measures ANOVA, Holm-Sidak *post hoc*.

rhythmic PD and LPG bursting via electrical coupling, from AB to PD and LPG, as well as between PD and LPG (Shruti et al., 2014; Marder et al., 2017; Zhang, Fahoum, Blitz, Nusbaum, unpublished). To test for a role of the pyloric network, we applied Gly[1]-SIFamide and injected hyperpolarizing current into each of the PD neurons to turn off pyloric pacemaker activity (Fig. 6). Because of the electrical coupling, hyperpolarization of the PDs sufficiently hyperpolarizes AB to eliminate rhythmic activity in all five pacemaker ensemble neurons (Bartos et al., 1999; Blitz et al., 2008). Shutting off rhythmic electrical synaptic input to LPG eliminated its pyloric-timed bursting but did not alter its most hyperpolarized membrane potential (PD On to Off: -51.5 ± 0.71 to -51.8 ± 0.91 mV, $n = 6$; $t_{(5)} = 0.336$, $p = 0.751$, paired t test), presumably because of the rectifying nature of this electrical coupling (Shruti et al., 2014).

Rhythmic pyloric network input was also not necessary for LPG to generate oscillations at a gastric mill frequency. We first verified in each experiment that Gly[1]-SIFamide (5×10^{-6} M) application elicited dual bursting in LPG with the pyloric rhythm on (Fig. 6*A*, left). We then hyperpolarized the two PD neurons to turn off the pyloric rhythm, eliminating pyloric bursting in LPG. However, LPG continued to generate gastric mill-timed bursts (Fig. 6*A*, right). Across experiments, in the absence of pyloric pacemaker activity, LPG generated gastric mill-timed bursting but failed to produce pyloric-timed bursts ($n = 9/9$) (Table 1; Fig. 6*B*). Based on a qualitative assessment of LPG activity during PD/PD hyperpolarization, the small amount of LPG activity that occurred within the spectral range of pyloric timing reflects spikes within gastric mill-timed bursts that are separated by the duration of a pyloric interval (~1 s) and not pyloric-timed bursts. To verify that LPG bursting when the pyloric rhythm was off was only gastric mill-timed, we quantified the cycle period and burst duration of fast and slow bursts when both networks were intact, and of isolated LPG bursts when rhythmic pyloric input was suppressed. Plotting the average cycle period versus burst duration, fast pyloric (red circles) and slow gastric mill (blue circles) bursts segregate into two distinct clusters (Fig. 6*C*). Across experiments, the isolated LPG bursts (Fig. 6*C*, gray circles) overlapped only with the LPG slow burst cluster and not with the fast burst cluster (Fig. 6*C*; $n = 9$). The inability to maintain pyloric-timed bursting indicates that AB continued to be a necessary pacemaker neuron for the pyloric rhythm and LPG was coactive with the pyloric rhythm because of electrical coupling. The ability of LPG to generate gastric mill-timed bursts without input from the pyloric pacemaker neurons or the gastric mill neurons (above) led us to test whether the gastric mill-timed bursting in LPG occurred entirely through intrinsic mechanisms.

LPG slow bursting occurs via intrinsic mechanisms

To ensure that there were no compensatory synaptic mechanisms supporting LPG bursting by one network when rhythmic input from the other one was eliminated, we tested whether the slow bursting elicited by Gly[1]-SIFamide, either exogenously applied or neuronally released by MCN5, occurred without rhythmic input from either network. In control Gly[1]-SIFamide application, LPG generated dual-network activity in pyloric and gastric mill time (Fig. 7*Ai*). We then isolated LPG from rhythmic gastric mill and pyloric input using PTX (10^{-5} M) application to block glutamatergic inhibitory chemical transmission plus PD/PD hyperpolarization (PTX:PD_{hype}). In these experiments, the LP neuron remained intact; however, its influence on LPG was blocked by PTX. Additionally, gastric mill neurons LG, Int1, DG, IC, and MG use glutamatergic inhibition within the STG, which is blocked by PTX (Marder and Eisen, 1984). During Gly[1]-SIFamide application, the isolated LPG still generated bursts (Fig. 7*Aii*) with a shift to a higher percent gastric mill-timed activity across experiments (Fig. 7*C*) (SIF: $31.40 \pm 9.35\%$; SIF:PTX:PD_{hype}: $78.28 \pm 7.20\%$, $n = 5$, $t_{(4)} = -7.399$, $p = 0.002$, paired t test). MCN5 stimulation also elicited dual-network activity in control conditions (Fig. 7*Bi*) and only slow bursting in the isolated condition (PTX:PD_{hype}) (Fig. 7*Bii*), with a greater percent gastric mill activity across experiments (Fig. 7*C*) (MCN5: $47.06 \pm 6.50\%$; MCN5:PTX:PD_{hype}: 69.40 ± 3.48, $n = 4$, $t_{(3)} = -6.415$, $p = 0.008$, paired t test). Similar to the spectral analysis in Figure 6, the remaining pyloric component in the spectral analysis does not match our qualitative assessment that there were no pyloric-timed bursts. To confirm that the LPG activity consisted of only slower, gastric mill-timed bursts, we again plotted cycle period against burst duration. Once again, the isolated LPG bursts (gray circles) overlapped with the gastric mill-timed LPG burst cluster (blue circles) and not the pyloric-timed burst cluster (red circles) for both Gly[1]-SIFamide (filled circles, $n = 5$) and MCN5 stimulation (open circles, $n = 4$; Fig. 7*D*). These data

indicate that the LPG dual-network activity includes fast pyloric bursting via electrical coupling, but slower gastric mill-timed bursting via intrinsic properties. If the slower LPG bursting is intrinsically generated, it should be voltage-dependent (Hablitz and Johnston, 1981; Adams and Benson, 1985; Marder and Calabrese, 1996).

We used PTX:PD_{hype} to isolate LPG from both networks and current injections to manipulate LPG membrane potential to examine whether Gly^1-SIFamide (5×10^{-6} M)-elicited LPG bursting was voltage-dependent. As above, the LP neuron was intact, but its actions blocked by PTX. In an example experiment, at baseline conditions (0 nA), LPG was bursting with a cycle period of 28 s and a duty cycle of 27% (Fig. 8*Ai*). Duty cycle is the percentage of a cycle during which a neuron is active. Depolarization of LPG (1 nA) noticeably increased LPG burst duration, with a smaller effect on cycle period (22 s), resulting in an increased duty cycle (70%). A further depolarization (1.5 nA) resulted in tonic firing, although there was still some visible regulation of firing rate (Fig. 8*Ai*). Hyperpolarizing LPG (−1 nA) decreased burst duration and increased cycle period (43 s), thus decreasing duty cycle (6%). Further hyperpolarization (−2 nA) eliminated LPG bursting (Fig. 8*Ai*). eEPSPs in the LPG intracellular trace are from the other LPG neuron, as these two neurons are electrically coupled (Weimann et al., 1991). To confirm that the oscillations are intrinsic to each LPG and do not require the electrical coupling between them, in two preparations we photoinactivated (see Materials and Methods) one LPG neuron and recorded from the one remaining LPG. In both cases, LPG generated oscillations in isolation from rhythmic pyloric and gastric mill input (Fig. 8*Aii*). These oscillations were again voltage-dependent, as they increased in burst duration with depolarization until LPG fired tonically and exhibited an increased cycle period plus decreased burst duration with hyperpolarization (Fig. 8*Aii*; $n = 2$). Across multiple experiments, the LPG cycle period increased with hyperpolarizing current injections and increased with depolarizing current injections (Fig. 8*B*; $n = 6$ with two LPGs intact). This parabolic relationship of cycle period with voltage occurs in other intrinsically bursting neurons based on the balance of inward and outward conductances (Skinner et al., 1993; Selverston et al., 2009). Bursting was eliminated (gray bars) with sufficiently hyperpolarizing current injections (−1 nA, $n = 1/6$; −1.5 nA, $n = 1/6$; −2 nA, $n = 4/6$) (Fig. 8*B*). LPG fired tonically (white bar) based on our burst criteria (see Materials and Methods), such that there were no ISIs longer than a typical pyloric cycle with depolarizing current injections (1.5 nA, $n = 3/6$), or when it did not fire tonically, LPG was bursting at the highest current injections where the recording was still stable (1 nA, $n = 1/6$; 1.5 nA, $n = 2/6$). LPG duty cycle decreased with hyperpolarizing current injection and increased with depolarizing current injection (Fig. 8*C*). Collectively, these data identify LPG slow gastric mill-timed bursting elicited by the modulatory actions of bath-applied and MCN5-released Gly^1-SIFamide as voltage-dependent, intrinsically generated.

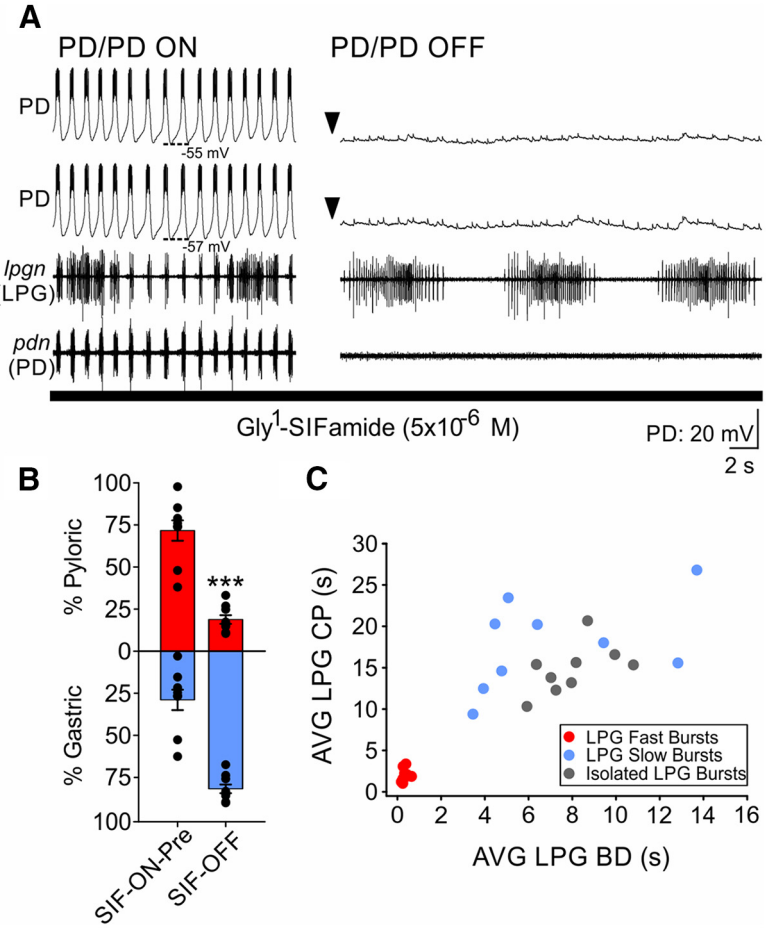

Figure 6. The Gly^1-SIFamide-elicited LPG switch to gastric mill-timed bursting does not require rhythmic input from the pyloric pacemaker ensemble. ***A***, Left, Gly^1-SIFamide (5×10^{-6} M) bath application elicited dual-network activity in LPG (*lpgn*) with the pyloric pacemaker neurons (AB, PD, PD) active. Right, During the Gly^1-SIFamide application, each of the two PD neurons was hyperpolarized (−4 nA; downward arrowheads), which also hyperpolarized the AB neuron (data not shown; see Materials and Methods) and eliminated rhythmic pyloric-timed activity in the entire pacemaker ensemble, including LPG. However, LPG continued to produce slow, gastric mill-timed bursting. Neurons were recorded with an unbalanced bridge; and hyperpolarized traces are aligned for ease of visualization, not to represent actual membrane potentials. ***B***, LPG activity was analyzed with spectral analysis and converted to a percentage pyloric- (red) and gastric mill- (blue) timed activity. During PD neuron hyperpolarization and elimination of the rhythmic pyloric pacemaker activity (SIF-OFF), there was more gastric mill-timed LPG activity compared with before (SIF-ON-Pre) PD hyperpolarization. ***$p < 0.001$ (one-way repeated-measures ANOVA, Holm-Sidak *post hoc*; see Table 1). ***C***, The average cycle period (CP) and burst duration (BD) are plotted for fast LPG bursts (red dots) and slow LPG bursts (blue dots) during the SIF-ON-Pre condition and for isolated LPG bursts (gray dots) during the SIF-OFF condition. The cycle period and burst duration of LPG bursts when it is isolated from rhythmic pyloric input overlap with the slow burst cluster, not the fast burst cluster. Each dot is the average of each type of burst from a single experiment, with 1 red, 1 blue, and 1 gray dot per experiment ($n = 9$). There appear to be fewer red dots because of the overlap of several dots.

Discussion

We identified a novel mechanism of switching a neuron from single- to dual-network participation. Specifically, modulating intrinsic membrane properties enables neuronal switching into bursting at a second network frequency (LPG, gastric mill rhythm), while electrical synapses maintain switching neuron activity in its "home" network (LPG, pyloric rhythm).

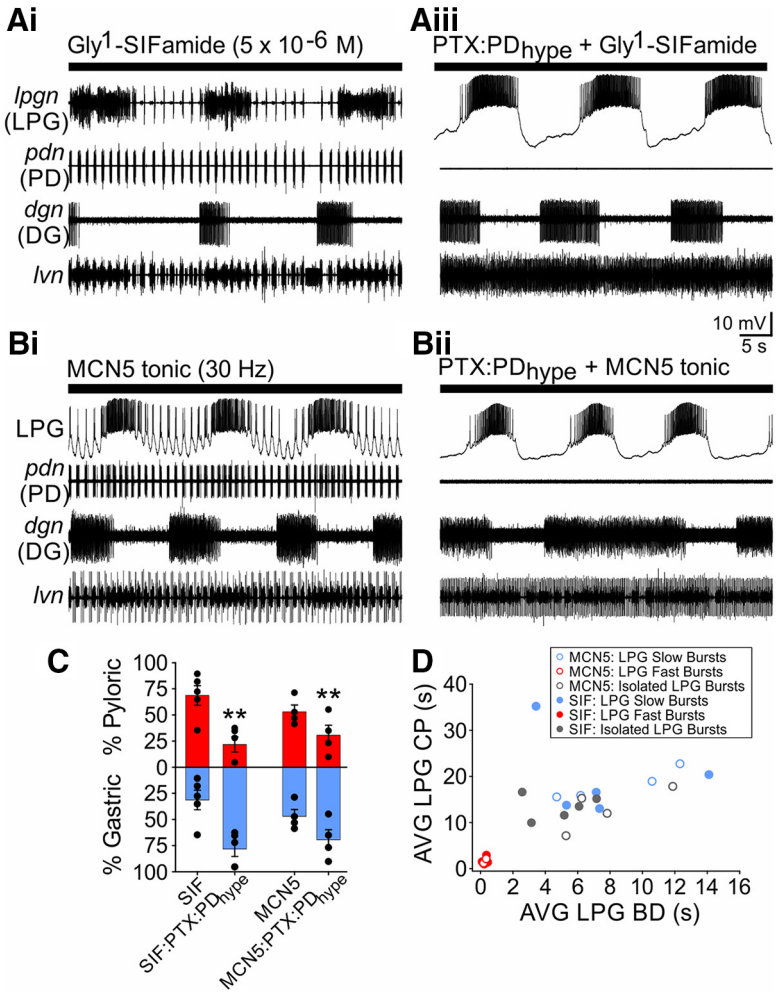

Figure 7. LPG gastric mill-timed bursting can be elicited by exogenous Gly^1-SIFamide or MCN5 stimulation, in the absence of any rhythmic pyloric or gastric mill network input. ***Ai***, Bath-applied Gly^1-SIFamide (5×10^{-6} M) elicited rhythmic bursting in the gastric mill neuron DG (*dgn*) and dual bursting activity in LPG (*lpgn*). ***Aii***, PTX (10^{-5} M) was used to block glutamatergic inhibition from the LP neuron and the gastric mill network, and the two PD neurons were hyperpolarized (PTX:PD$_{hype}$) to eliminate rhythmic pyloric activity (*pdn*). In this isolated condition, the LPG neuron was still able to generate slow bursts during Gly^1-SIFamide application. The efficacy of PTX is evident in the overlapping LP/PY activity in the *lvn* recording. LPG was recorded extracellularly (***Ai***) before an intracellular recording was obtained later in the experiment (***Aii***). MCN5 also elicited dual bursting in LPG during control conditions (***Bi***) and only slow bursting in PTX (10^{-5} M) with the two PD neurons hyperpolarized (***Bii***). ***C***, Spectral analysis indicates that there was a difference between LPG slow bursting and isolated LPG bursts in Gly^1-SIFamide versus Gly^1-SIFamide + PTX:PD$_{hype}$, and during MCN5 stimulation versus MCN5 + PTX:PD$_{hype}$. $^{**}p < 0.01$ (paired *t* test). ***D***, To verify that the single-frequency LPG bursting in the isolated condition was gastric mill-timed bursting, the average cycle period (CP) and burst duration (BD) were plotted for pyloric and gastric mill LPG bursts in control conditions, and for isolated LPG bursts. The isolated LPG bursts (Gly^1-SIFamide, filled gray circles; MCN5, open gray circles) overlap with control condition gastric mill slow bursts (Gly^1-SIFamide, filled blue circles; MCN5, open blue circles) and not with pyloric bursts (Gly^1-SIFamide, filled red circles; MCN5, open red circles). Gly^1-SIFamide ($n = 5$); MCN5 ($n = 4$).

Neuronal switching

Network flexibility includes neuronal switching, in which neurons change their network participation via neuromodulatory inputs. This includes switching between networks (Hooper and Moulins, 1990; Ramirez, 1998; Jean, 2001), merging multiple networks, or novel networks forming from participants of multiple networks (Dickinson et al., 1990; Weimann et al., 1991; Meyrand et al., 1994; Faumont et al., 2005). Behaviorally related networks are often coactive, and neurons can participate in multiple oscillatory networks simultaneously (Weimann et al., 1991; Steriade et al., 1993; Larson et al., 1994; Bucher et al., 2006; Jacobs et al., 2007; Rangel et al., 2016). However, dual-network activity is flexible; thus, single-to-dual-network switching also occurs (Dickinson, 1995; Gestreau et al., 2000; Tryba et al., 2008; Bartlett and Leiter, 2012; Schmidt and Wild, 2014).

Mechanisms of neuronal switching

Before this study, the identified mechanism for recruiting switching neurons into another network, or into dual-network activity, was modulation of synaptic strength. For example, in lobster STNS networks, different neuromodulatory inputs alter synaptic strength to recruit a pyloric neuron into the cardiac sac network (Hooper and Moulins, 1990), or to recruit pyloric, gastric mill, and oesophageal network neurons into one network to produce a novel rhythm (Meyrand et al., 1994).

Although synaptic modulation is essential to neuronal switching, modulation of intrinsic membrane properties can contribute to neurons leaving a network. For example, while synaptic modulation recruits STNS neurons into networks, modulation of intrinsic properties removes neurons from their home networks (Cazalets et al., 1990; Hooper and Moulins, 1990; Faumont et al., 2005). Additionally, intrinsic property modulation may play a primary role when an exogenous neuromodulator causes dual sigh/eupneic mouse respiratory neurons to leave the eupneic network, despite fast chemical synaptic transmission being blocked (Tryba et al., 2008). However, the inability to simultaneously monitor all, or completely isolate individual neurons in the relatively large respiratory network, raises the possibility that another mechanism, such as electrical synapse modulation, may underlie dual-to-single-network switching (Tryba et al., 2008). Further, intrinsic property modulation may serve a primary role in neuronal switching, even with unmodulated synapses (Drion et al., 2019).

In our study, it was possible that gastric mill network, or pyloric electrical synaptic input (albeit at a different frequency), or both, was necessary for switching LPG into dual-frequency oscillations. In a computational study, modulation of both electrical and chemical synaptic strength facilitates neuronal switching (Gutierrez et al., 2013). The small pyloric/gastric mill networks enabled us to determine that, for both exogenously applied and endogenously MCN5-released Gly^1-SIFamide, LPG did not require synaptic input to generate voltage-dependent oscillations at a second frequency. Thus, intrinsic property modulation, without a synaptic component, enables a neuron to generate oscillations at a second frequency timed with a second network.

Modulating intrinsic instead of synaptic properties to enable dual-frequency bursting has potential consequences for network function. First, a strengthened synapse imposing another frequency onto a neuron implies a passive role of this switching

neuron in the new network. However, when the switching neuron intrinsically generates the appropriate frequency bursting, it could contribute to rhythm generation in the new network. In control, LPG is part of the pyloric pacemaker ensemble (Marder and Bucher, 2007), whereas in the MCN5/Gly^1-SIFamide state, it may contribute to rhythm generation for two networks, at two distinct frequencies. Second, when synaptic modulation "pulls" a switching neuron into another network, the enhanced synapse enables both appropriately timed bursting and coordination with network neurons. However, modulating intrinsic properties to elicit neuronal switching at the appropriate frequency is independent from coordination. In addition to LPG to DG, synapses capable of coordinating LPG and gastric mill neurons are not yet identified (Marder and Bucher, 2007). However, synapses in this and many other systems are subject to extensive modulation (Harris-Warrick, 2011; Nadim and Bucher, 2014). Thus, MCN5/Gly^1-SIFamide likely modulate synapses along with LPG intrinsic properties. Separating the two components of neuronal switching enables independent regulation and may allow for switching neurons to actively contribute to coordination in the new network. We have not yet determined the modulatory actions responsible for coordination in the MCN5/Gly^1-SIFamide gastric mill rhythm.

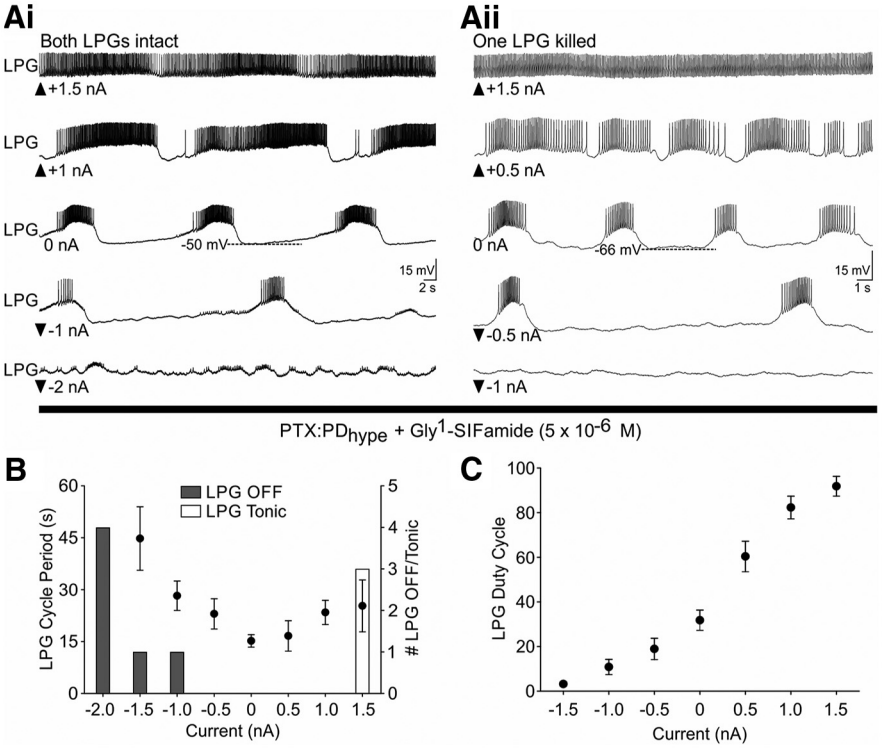

Figure 8. LPG gastric mill-timed bursting is voltage-dependent. ***Ai***, Several current injection levels are shown for an example LPG neuron during PTX:PD$_{hype}$ and Gly^1-SIFamide application with both LPGs intact. Depolarizing current injections (upward-facing arrowheads) increased LPG burst duration (1 nA) or elicited tonic firing (1.5 nA). Activity was considered to be tonic when there were no ISIs longer than a typical pyloric cycle. Hyperpolarizing current injections (downward-facing arrowheads) increased cycle period and decreased burst duration (−1 nA) or eliminated bursting (−2 nA). ***Aii***, One LPG was photoinactivated (killed; see Materials and Methods) and the remaining LPG subjected to depolarizing and hyperpolarizing current injections during PTX:PD$_{hype}$ and Gly^1-SIFamide application. Similar to when both LPGs were intact, depolarizing current (0.5 nA) increased burst duration or elicited tonic firing (1.5 nA) and hyperpolarizing current injection slowed (−0.5 nA) or eliminated (−1 nA) bursting. ***Ai*** and ***Aii*** are from separate preparations. ***B***, The average LPG cycle period across experiments is plotted as a function of current injection (circles ± error bars). The number of preparations in which LPG bursting turned off (gray bars) or became tonic (white bar) is plotted on the same graph ($n = 6$). ***C***, LPG duty cycle, the percentage of a cycle that a neuron is active, is plotted as a function of current injection. LPG duty cycle decreased with hyperpolarizing current injection and increased with depolarizing current injection. Bursting parameters are the average of 2-5 cycles at each current injection (see Materials and Methods) for preparations with both LPGs intact ($n = 6$).

Interactions between synaptic and intrinsic properties

Although commonly known for synchronization, electrical synapses can have complex interactions with chemical synapses and intrinsic properties, and thus unexpected consequences for network output (Weaver et al., 2010; Connors, 2017; Jing et al., 2017; Marder et al., 2017; Nadim et al., 2017; Alcamí and Pereda, 2019). For example, electrical coupling enables rapid switches in network output among neurons connected via chemical synapses (Bem et al., 2005), a larger range of network outputs, and switching between networks oscillating at distinct frequencies (Gutierrez and Marder, 2014). Here, electrical coupling maintaining LPG activity in the pyloric network must be balanced with slow burst intrinsic currents eliciting periodic LPG escapes from the pyloric network. This balance may require MCN5/Gly^1-SIFamide to decrease LPG-PD/AB coupling strength. Similar to chemical synapses, electrical synapses are highly modulated, including direct modulation of gap junction channels (Zsiros and Maccaferri, 2008; Lane et al., 2016), or indirect effects on functional coupling through modulation of ionic conductances (Szabo et al., 2010; Haas and Landisman, 2012; Nadim et al., 2017). Either MCN5 cotransmitter Gly^1-SIFamide or glutamate (Blitz et al., 2019; present study) could modulate electrical synapses. MCN5-released glutamate acts via fast ionotropic inhibition but may also target metabotropic glutamate receptors in STG neurons (Krenz et al., 2000) to modulate electrical synapses, as in other systems (Curti and O'Brien, 2016). Although biogenic amine modulation of electrical coupling is well described (Johnson et al., 1994; Zsiros and Maccaferri, 2008; Szabo et al., 2010), peptide regulation of electrical transmission does occur (Wang et al., 2014; Cachope and Pereda, 2015). Such modulatory actions may directly alter LPG gap junctions or change the functional impact of LPG-PD/AB coupling because of MCN5/Gly^1-SIFamide modulation of intrinsic properties underlying LPG slow bursting.

It is also possible that gap junction properties facilitate interactions between electrical synapses and intrinsic properties important for switching. For instance, pyloric pacemaker electrical synapses are rectifying, with depolarizing current flowing preferentially from PD/AB to LPG, and hyperpolarizing current from LPG to PD/AB neurons (Fig. 1*B*) (Shruti et al., 2014). Thus, intrinsic current(s) initiating LPG slow bursts may overcome electrical coupling because the rectification decreases electrical synaptic current as LPG depolarizes above PD/AB membrane potentials. Contributions of rectification to network output are likely underappreciated, as its identification requires directly recording from, and manipulating, coupled neurons. However,

they can play important functions within circuits, such as regulating network sensitivity to chemical synaptic input (Gutierrez and Marder, 2013; O'Brien, 2014; Palacios-Prado et al., 2014; Szczupak, 2016). Voltage-dependent burst currents might also shunt electrical coupling to prevent it from interrupting LPG slow bursts, but these possibilities have not yet been explored.

Functional implications of neuronal switching

Rhythmic behaviors, such as respiration and locomotion, swallowing and vocalization, and feeding-related behaviors, require coordination (Bernasconi and Kohl, 1993; Wood et al., 2004; Bartlett and Leiter, 2012). Indeed, there are dangerous consequences to poor coordination, such as aspiration with improper swallowing/breathing coordination (Bartlett and Leiter, 2012). Furthermore, individual muscles can alternate between different rhythmic behaviors, or contribute to multiple simultaneous behaviors (Lancaster et al., 1995; Ramirez, 1998; Gestreau et al., 2000; Schmidt and Wild, 2014). However, the extent of coordination varies based on behavioral version or environmental conditions (Lancaster et al., 1995; Stickford and Stickford, 2014; Stein and Harzsch, 2021). Neuronal switching between single- and dual-network activity may underlie such flexibility for network coordination.

Beyond rhythmic motor networks, systems-level studies suggest that neuromodulatory inputs elicit rapid reconfiguration of oscillatory networks involved in sensory and cognitive processes (Draguhn and Buzsáki, 2004; Roopun et al., 2008; Haider and McCormick, 2009; Ainsworth et al., 2011; Akam and Kullmann, 2014; Rangel et al., 2016). Specifically, a suggested major role of noradrenergic locus coeruleus neurons is large-scale, brain-wide network reconfiguration (Bouret and Sara, 2005; Grella et al., 2019), supported by fMRI studies in mice and humans (Hermans et al., 2011; Zerbi et al., 2019). In nonmotor networks, it can be difficult to identify behavioral consequences of changing coactivation across brain regions. Potential functions of rapid network reorganization, including switching between single and multiple oscillatory frequencies, include combining multimodal aspects of sensory perception, or multiple components of a memory for storage (Roopun et al., 2008; Wang, 2010; Akam and Kullmann, 2014). Dysfunction in these processes may lead to neurologic disorders, suggested by decreased synchrony between brain regions in schizophrenia patients, and brain network dysregulation, potentially because of locus coeruleus changes, in autism spectrum disorders (Uhlhaas and Singer, 2010; London, 2018). Given the many similarities in network function and plasticity from small to large networks (Haider and McCormick, 2009; Koch et al., 2011; Bargmann and Marder, 2013; Kopell et al., 2014), similar basic principles of neuronal switching in small networks will likely extend to larger, more diffuse networks.

References

Adams WB, Benson JA (1985) The generation and modulation of endogenous rhythmicity in the *Aplysia* bursting pacemaker neurone R15. Prog Biophys Mol Biol 46:1–49.

Ainsworth M, Lee S, Cunningham MO, Roopun AK, Traub RD, Kopell NJ, Whittington MA (2011) Dual gamma rhythm generators control interlaminar synchrony in auditory cortex. J Neurosci 31:17040–17051.

Akam T, Kullmann DM (2014) Oscillatory multiplexing of population codes for selective communication in the mammalian brain. Nat Rev Neurosci 15:111–122.

Alcamí P, Pereda AE (2019) Beyond plasticity: the dynamic impact of electrical synapses on neural circuits. Nat Rev Neurosci 20:253–271.

Bargmann CI, Marder E (2013) From the connectome to brain function. Nat Methods 10:483–490.

Bartlett D, Leiter JC (2012) Coordination of breathing with nonrespiratory activities. Compr Physiol 2:1387–1415.

Bartos M, Nusbaum MP (1997) Intercircuit control of motor pattern modulation by presynaptic inhibition. J Neurosci 17:2247–2256.

Bartos M, Manor Y, Nadim F, Marder E, Nusbaum MP (1999) Coordination of fast and slow rhythmic neuronal circuits. J Neurosci 19:6650–6660.

Beenhakker MP, Blitz DM, Nusbaum MP (2004) Long-lasting activation of rhythmic neuronal activity by a novel mechanosensory system in the crustacean stomatogastric nervous system. J Neurophysiol 91:78–91.

Bem T, Le Feuvre Y, Rinzel J, Meyrand P (2005) Electrical coupling induces bistability of rhythms in networks of inhibitory spiking neurons. Eur J Neurosci 22:2661–2668.

Bernasconi P, Kohl J (1993) Analysis of co-ordination between breathing and exercise rhythms in man. J Physiol 471:693–706.

Bidaut M (1980) Pharmacological dissection of pyloric network of the lobster stomatogastric ganglion using picrotoxin. J Neurophysiol 44:1089–1101.

Blitz DM, Beenhakker MP, Nusbaum MP (2004) Different sensory systems share projection neurons but elicit distinct motor patterns. J Neurosci 24:11381–11390.

Blitz DM, White RS, Saideman SR, Cook A, Christie AE, Nadim F, Nusbaum MP (2008) A newly identified extrinsic input triggers a distinct gastric mill rhythm via activation of modulatory projection neurons. J Exp Biol 211:1000–1011.

Blitz DM, Christie AE, Cook AP, Dickinson PS, Nusbaum MP (2019) Similarities and differences in circuit responses to applied Gly^1-SIFamide and peptidergic (Gly^1-SIFamide) neuron stimulation. J Neurophysiol 121:950–972.

Bouret S, Sara SJ (2005) Network reset: a simplified overarching theory of locus coeruleus noradrenaline function. Trends Neurosci 28:574–582.

Bucher D, Haspel G, Golowasch J, Nadim F (2015) Central pattern generators. Chichester: Wiley.

Bucher D, Taylor AL, Marder E (2006) Central pattern generating neurons simultaneously express fast and slow rhythmic activities in the stomatogastric ganglion. J Neurophysiol 95:3617–3632.

Buzsáki G (2002) Theta oscillations in the hippocampus. Neuron 33:325–340.

Cachope R, Pereda AE (2015) Opioids potentiate electrical transmission at mixed synapses on the Mauthner cell. J Neurophysiol 114:689–697.

Cazalets JR, Nagy F, Moulins M (1990) Suppressive control of the crustacean pyloric network by a pair of identified interneurons: I. Modulation of the motor pattern. J Neurosci 10:458–468.

Cleland TA, Selverston AI (1995) Glutamate-gated inhibitory currents of central pattern generator neurons in the lobster stomatogastric ganglion. J Neurosci 15:6631–6639.

Coleman MJ, Nusbaum MP (1994) Functional consequences of compartmentalization of synaptic input. J Neurosci 14:6544–6552.

Coleman MJ, Meyrand P, Nusbaum MP (1995) A switch between two modes of synaptic transmission mediated by presynaptic inhibition. Nature 378:502–505.

Connors BW (2017) Synchrony and so much more: diverse roles for electrical synapses in neural circuits. Dev Neurobiol 77:610–624.

Curti S, O'Brien J (2016) Characteristics and plasticity of electrical synaptic transmission. BMC Cell Biol 17:13.

Daur N, Nadim F, Bucher D (2016) The complexity of small circuits: the stomatogastric nervous system. Curr Opin Neurobiol 41:1–7.

Dickinson PS (1995) Interactions among neural networks for behavior. Curr Opin Neurobiol 5:792–798.

Dickinson PS, Mecsas C, Marder E (1990) Neuropeptide fusion of two motor-pattern generator circuits. Nature 344:155–157.

Dickinson PS, Stemmler EA, Cashman CR, Brennan HR, Dennison B, Huber KE, Peguero B, Rabacal W, Goiney CC, Smith CM, Towle DW, Christie AE (2008) SIFamide peptides in clawed lobsters and freshwater crayfish (*Crustacea*, *Decapoda*, *Astacidea*): a combined molecular, mass spectrometric and electrophysiological investigation. Gen Comp Endocrinol 156:347–360.

Draguhn A, Buzsáki G (2004) Neuronal oscillations in cortical networks. Science 304:1926–1930.

Drion G, Franci A, Sepulchre R (2019) Cellular switches orchestrate rhythmic circuits. Biol Cybern 113:71–82.

Faumont S, Combes D, Meyrand P, Simmers J (2005) Reconfiguration of multiple motor networks by short- and long-term actions of an identified modulatory neuron. Eur J Neurosci 22:2489–2502.

Gestreau C, Grélot L, Bianchi AL (2000) Activity of respiratory laryngeal motoneurons during fictive coughing and swallowing. Exp Brain Res 130:27–34.

Graubard K, Hartline DK (1987) Full-wave rectification from a mixed electrical-chemical synapse. Science 237:535–537.

Grella SL, Neil JM, Edison HT, Strong VD, Odintsova IV, Walling SG, Martin GM, Marrone DF, Harley CW (2019) Locus coeruleus phasic, but not tonic, activation initiates global remapping in a familiar environment. J Neurosci 39:445–455.

Gutierrez GJ, Grashow RG (2009) *Cancer borealis* stomatogastric nervous system dissection. J Vis Exp 25:1207.

Gutierrez GJ, Marder E (2013) Rectifying electrical synapses can affect the influence of synaptic modulation on output pattern robustness. J Neurosci 33:13238–13248.

Gutierrez GJ, Marder E (2014) Modulation of a single neuron has state-dependent actions on circuit dynamics. eNeuro 1:ENEURO.0009-14.2014.

Gutierrez GJ, O'Leary T, Marder E (2013) Multiple mechanisms switch an electrically coupled, synaptically inhibited neuron between competing rhythmic oscillators. Neuron 77:845–858.

Haas JS, Landisman CE (2012) State-dependent modulation of gap junction signaling by the persistent sodium current. Front Cell Neurosci 5:31.

Hablitz JJ, Johnston D (1981) Endogenous nature of spontaneous bursting in hippocampal pyramidal neurons. Cell Mol Neurobiol 1:325–334.

Haider B, McCormick DA (2009) Rapid neocortical dynamics: cellular and network mechanisms. Neuron 62:171–189.

Harris-Warrick RM (2011) Neuromodulation and flexibility in central pattern generator networks. Curr Opin Neurobiol 21:685–692.

Hedrich UB, Diehl F, Stein W (2011) Gastric and pyloric motor pattern control by a modulatory projection neuron in the intact crab *Cancer pagurus*. J Neurophysiol 105:1671–1680.

Hermans EJ, Van Marle HJ, Ossewaarde L, Henckens MJ, Qin S, Van Kesteren MT, Schoots VC, Cousijn H, Rijpkema M, Oostenveld R, Fernández G (2011) Stress-related noradrenergic activity prompts large-scale neural network reconfiguration. Science 334:1151–1153.

Hooper SL, Moulins M (1990) Cellular and synaptic mechanisms responsible for a long-lasting restructuring of the lobster pyloric network. J Neurophysiol 64:1574–1589.

Hooper SL, Thuma JB, Guschlbauer C, Schmidt J, Büschges A (2015) Cell dialysis by sharp electrodes can cause nonphysiological changes in neuron properties. J Neurophysiol 114:1255–1271.

Huybrechts J, Nusbaum MP, Bosch LV, Baggerman G, De Loof A, Schoofs L (2003) Neuropeptidomic analysis of the brain and thoracic ganglion from the Jonah crab, *Cancer borealis*. Biochem Biophys Res Commun 308:535–544.

Jacobs J, Kahana MJ, Ekstrom AD, Fried I (2007) Brain oscillations control timing of single-neuron activity in humans. J Neurosci 27:3839–3844.

Jean A (2001) Brain stem control of swallowing: neuronal network and cellular mechanisms. Physiol Rev 81:929–969.

Jing J, Cropper EC, Weiss KR (2017) Network functions of electrical coupling present in multiple and specific sites in behavior-generating circuits. In: Network functions and plasticity: perspectives from studying neuronal electrical coupling in microcircuits, pp 79–107. Elsevier: Amstersdam.

Johnson BR, Peck JH, Harris-Warrick RM (1994) Differential modulation of chemical and electrical components of mixed synapses in the lobster stomatogastric ganglion. J Comp Physiol A Neuroethol Sens Neural Behav Physiol 175:233–249.

Koch H, Garcia AJ, Ramirez JM (2011) Network reconfiguration and neuronal plasticity in rhythm-generating networks. Integr Comp Biol 51:856–868.

Kopell NJ, Gritton HJ, Whittington MA, Kramer MA (2014) Beyond the connectome: the dynome. Neuron 83:1319–1328.

Krenz WD, Nguyen D, Pérez-Acevedo NL, Selverston AI (2000) Group I, II, and III mGluR compounds affect rhythm generation in the gastric circuit of the crustacean stomatogastric ganglion. J Neurophysiol 83:1188–1201.

Lancaster WC, Henson OW, Keating AW (1995) Respiratory muscle activity in relation to vocalization in flying bats. J Exp Biol 198:175–191.

Lane BJ, Samarth P, Ransdell JL, Nair SS, Schulz DJ (2016) Synergistic plasticity of intrinsic conductance and electrical coupling restores synchrony in an intact motor network. eLife 5:e16879.

Larson CR, Yajima Y, Ko P (1994) Modification in activity of medullary respiratory-related neurons for vocalization and swallowing. J Neurophysiol 71:2294–2304.

London EB (2018) Neuromodulation and a reconceptualization of autism spectrum disorders: using the locus coeruleus functioning as an exemplar. Front Neurol 9:1120.

Mamiya A, Manor Y, Nadim F (2003) Short-term dynamics of a mixed chemical and electrical synapse in a rhythmic network. J Neurosci 23:9557–9564.

Marder E (2012) Neuromodulation of neuronal circuits: back to the future. Neuron 76:1–11.

Marder E, Bucher D (2007) Understanding circuit dynamics using the stomatogastric nervous system of lobsters and crabs. Annu Rev Physiol 69:291–316.

Marder E, Calabrese RL (1996) Principles of rhythmic motor pattern generation. Physiol Rev 76:687–717.

Marder E, Eisen JS (1984) Transmitter identification of pyloric neurons: electrically coupled neurons use different transmitters. J Neurophysiol 51:1345–1361.

Marder E, O'Leary T, Shruti S (2014) Neuromodulation of circuits with variable parameters: single neurons and small circuits reveal principles of state-dependent and robust neuromodulation. Annu Rev Neurosci 37:329–346.

Marder E, Gutierrez GJ, Nusbaum MP (2017) Complicating connectomes: electrical coupling creates parallel pathways and degenerate circuit mechanisms. Dev Neurobiol 77:597–609.

McCormick DA, Bal T (1997) Sleep and arousal: thalamocortical mechanisms. Annu Rev Neurosci 20:185–215.

Meyrand P, Simmers J, Moulins M (1994) Dynamic construction of a neural network from multiple pattern generators in the lobster stomatogastric nervous system. J Neurosci 14:630–644.

Miller JP, Selverston AI (1979) Rapid killing of single neurons by irradiation of intracellularly injected dye. Science 206:702–704.

Nadim F, Bucher D (2014) Neuromodulation of neurons and synapses. Curr Opin Neurobiol 29:48–56.

Nadim F, Li X, Gray M, Golowasch J (2017) The role of electrical coupling in rhythm generation in small networks. In: Network functions and plasticity: perspectives from studying neuronal electrical coupling in microcircuits, pp 51–78. Elsevier: Amsterdam.

Norris BJ, Coleman MJ, Nusbaum MP (1996) Pyloric motor pattern modification by a newly identified projection neuron in the crab stomatogastric nervous system. J Neurophysiol 75:97–108.

Nusbaum MP, Beenhakker MP (2002) A small-systems approach to motor pattern generation. Nature 417:343–350.

O'Brien J (2014) The ever-changing electrical synapse. Curr Opin Neurobiol 29:64–72.

Palacios-Prado N, Huetteroth W, Pereda AE (2014) Hemichannel composition and electrical synaptic transmission: molecular diversity and its implications for electrical rectification. Front Cell Neurosci 8:1–13.

Ramirez JM (1998) Reconfiguration of the respiratory network at the onset of locust flight. J Neurophysiol 80:3137–3147.

Rangel LM, Rueckemann JW, Riviere PD, Keefe KR, Porter BS, Heimbuch IS, Budlong CH, Eichenbaum H (2016) Rhythmic coordination of hippocampal neurons during associative memory processing. eLife 5:e09849.

Rehm KJ, Taylor AL, Pulver SR, Marder E (2008) Spectral analyses reveal the presence of adult-like activity in the embryonic stomatogastric motor patterns of the lobster, *Homarus americanus*. J Neurophysiol 99:3104–3122.

Roopun AK, Kramer MA, Carracedo LM, Kaiser M, Davies CH, Traub RD, Kopell NJ, Whittington MA (2008) Temporal interactions between cortical rhythms. Front Neurosci 2:145–154.

Schmidt MF, Wild JM (2014) The respiratory-vocal system of songbirds: anatomy, physiology, and neural control. Prog Brain Res 212:297–335.

Selverston AI, Szücs A, Huerta R, Pinto R, Reyes M (2009) Neural mechanisms underlying the generation of the lobster gastric mill motor pattern. Front Neural Circuits 3:12–23.

Shruti S, Schulz DJ, Lett KM, Marder E (2014) Electrical coupling and innexin expression in the stomatogastric ganglion of the crab *Cancer borealis*. J Neurophysiol 112:2946–2958.

Skinner FK, Turrigiano GG, Marder E (1993) Frequency and burst duration in oscillating neurons and two-cell networks. Biol Cybern 69:375–383.

Stein W (2009) Modulation of stomatogastric rhythms. J Comp Physiol A Neuroethol Sens Neural Behav Physiol 195:989–1009.

Stein W, Harzsch S (2021) The neurobiology of ocean change: insights from decapod crustaceans. Zoology (Jena) 144:125887.

Steriade M, Nunez A, Amzica F (1993) Intracellular analysis of relations between the slow (<1 Hz) neocortical oscillation and other sleep rhythms of the electroencephalogram. J Neurosci 13:3266–3283.

Stickford AS, Stickford JL (2014) Ventilation and locomotion in humans: mechanisms, implications, and perturbations to the coupling of these two rhythms. Springer Sci Rev 2:95–118.

Szabo TM, Caplan JS, Zoran MJ (2010) Serotonin regulates electrical coupling via modulation of extrajunctional conductance: h-current. Brain Res 1349:21–31.

Szczupak L (2016) Functional contributions of electrical synapses in sensory and motor networks. Curr Opin Neurobiol 41:99–105.

Tryba AK, Peña F, Lieske SP, Viemari JC, Thoby-Brisson M, Ramirez JM (2008) Differential modulation of neural network and pacemaker activity underlying eupnea and sigh-breathing activities. J Neurophysiol 99:2114–2125.

Uhlhaas PJ, Singer W (2010) Abnormal neural oscillations and synchrony in schizophrenia. Nat Rev Neurosci 11:100–113.

Wang MH, Chen N, Wang JH (2014) The coupling features of electrical synapses modulate neuronal synchrony in hypothalamic superachiasmatic nucleus. Brain Res 1550:9–17.

Wang XJ (2010) Neurophysiological and computational principles of cortical rhythms in cognition. Physiol Rev 90:1195–1268.

Weaver AL, Roffman RC, Norris BJ, Calabrese RL (2010) A role for compromise: synaptic inhibition and electrical coupling interact to control phasing in the leech heartbeat CPG. Front Behav Neurosci 4:38.

Weimann JM, Marder E (1994) Switching neurons are integral members of multiple oscillatory networks. Curr Biol 4:896–902.

Weimann JM, Meyrand P, Marder E (1991) Neurons that form multiple pattern generators: identification and multiple activity patterns of gastric/pyloric neurons in the crab stomatogastric system. J Neurophysiol 65:111–122.

White RS, Nusbaum MP (2011) The same core rhythm generator underlies different rhythmic motor patterns. J Neurosci 31:11484–11494.

Wood DE, Manor Y, Nadim F, Nusbaum MP (2004) Intercircuit control via rhythmic regulation of projection neuron activity. J Neurosci 24:7455–7463.

Yasuda A, Yasuda-Kamatani Y, Nozaki M, Nakajima T (2004) Identification of GYRKPPFNGSIFamide (crustacean-SIFamide) in the crayfish *Procambarus clarkii* by topological mass spectrometry analysis. Gen Comp Endocrinol 135:391–400.

Zerbi V, Floriou-Servou A, Markicevic M, Vermeiren Y, Sturman O, Privitera M, von Ziegler L, Ferrari KD, Weber B, de Deyn PP, Wenderoth NN, Bohacek J (2019) Rapid reconfiguration of the functional connectome after chemogenetic locus coeruleus activation. Neuron 103:702–718.

Zsiros V, Maccaferri G (2008) Noradrenergic modulation of electrical coupling in GABAergic networks of the hippocampus. J Neurosci 28:1804–1815.